Journal of Structural Geology 42 (2012) 74–90

Contents lists available at SciVerse ScienceDirect

Journal of Structural Geology

journal homepage: www.elsevier.com/locate/jsg

Fabric evidence for granodiorite emplacement with extensional shear zones in the Variscan Gredos massif (Spanish Central System)

Juan Díaz-Alvarado [a], Carlos Fernández [a,*], Manuel Díaz-Azpiroz [b], Antonio Castro [c], Ignacio Moreno-Ventas [c]

[a] Departamento de Geodinámica y Paleontología, Universidad de Huelva, E-21071 Huelva, Spain
[b] Departamento de Sistemas Físicos, Químicos y Naturales, Universidad Pablo de Olavide, 41013 Seville, Spain
[c] Departamento de Geología, Universidad de Huelva, E-21071 Huelva, Spain

ARTICLE INFO

Article history:
Received 21 July 2011
Received in revised form
25 June 2012
Accepted 26 June 2012
Available online 6 July 2012

Keywords:
Magmatic fabric
SPO
Granodiorite
Deformation
Variscan belt

ABSTRACT

Three granitoid bodies in the central part of the Gredos massif (Spanish Central System batholith) are tabular, around 1 km in thickness, and intruded into a migmatitic middle crust during the D3 deformation phase of the Variscan Orogeny. Petrologically, they are composed of Bt-granodiorite and Crd-monzogranite, and they show varying abundance of large (cm-scale) feldspar megacrysts. A detailed study of the shape preferred orientation (SPO) magmatic fabric defined by these megacrysts, together with a kinematic analysis of the structures due to interactions between them, and the measurement of quartz *c*-axis fabrics in migmatites and granitoids, suggests that granitic magma and country rocks were mechanically coupled during deformation. The emplacement took place along large-scale, extensional shear zones active during the first stages of the D3 phase. The shape of the SPO ellipsoids varies from constrictional at the centre of the granitic bodies, to flattening or even oblate at their external contacts with the migmatitic host rocks. The favoured interpretation of this spatial fabric variation is the overprinting of the emplacement fabrics by a constrictional tectonic regime associated with the growth of tabular magma chambers along extensional detachments, followed by shear zone development commonly at the top of the granitic bodies. The entire structure was later folded during the last stages of the D3 phase.

1. Introduction

The study of the processes operating during the emplacement and structural evolution of the large masses of granitoid magmas in the continental crust has drawn the attention of petrologists and structural geologists since the pioneering work of Hans Cloos (e.g., Cloos, 1925). Considerable efforts during the second half of the past century identified the importance of the tectonic regime on the segregation, ascent and emplacement of granite magma (e.g., Brown, 1994; Bouchez et al., 1997; Brown and Solar, 1999; Castro et al., 1999; Petford et al., 2000; and references therein). The mechanical behaviour of magmas, the structure, kinematics and rheology of their host rocks, and the stress state of the crust were found to be essential parameters controlling the final shape of plutons and batholiths, and the generation and evolution of fabrics within them (e.g., Berger and Pitcher, 1970; Castro, 1987; Clemens and Mawer, 1992; D'Lemos et al., 1993; Petford et al., 1993; Brown, 1994; Collins and Sawyer, 1996; Clemens et al., 1997; Vigneresse et al., 1999; Petford, 2003; among many others).

Modern research about magmatic fabrics follows three main lines. First, the development and application of new techniques for the geometrical and kinematic characterisation of magmatic fabrics. This line includes the identification of the criteria to distinguish between magmatic and solid-state fabrics in granites (Paterson et al., 1989; Bouchez et al., 1992), the 2D and 3D determinations of shape fabrics (e.g., Launeau and Robin, 2005; Higgins, 2006), the application of AMS techniques (e.g., Jelinek, 1981; Bouchez, 1997), and the integrated use of classical field techniques, microstructural and geochronological studies (e.g., Kratinová et al., 2007). Numerical and analogue experiments are also now offering new perspectives on the development of magmatic fabrics and

* Corresponding author.
E-mail address: fcarlos@uhu.es (C. Fernández).

0191-8141/$ – see front matter © 2012 Elsevier Ltd. All rights reserved.
http://dx.doi.org/10.1016/j.jsg.2012.06.012

their kinematic implications (e.g., Fernandez and Fernández-Catuxo, 1997; Arbaret et al., 2000; Mulchrone et al., 2005; Jiang, 2007). The second research line is aimed at interpreting those fabrics. For instance, the criteria to establish the role that regional deformation plays in forming magmatic fabrics, early emphasised by Berger and Pitcher (1970), have been recently clarified through the use of the degree of structural continuity between pluton and host rock (Paterson et al., 1998; Wilson and Grocott, 1999; Kratinová et al., 2007). General agreement exists that magmatic fabrics form late in the crystallisation history, reflecting emplacement-level deformation (Wilson and Grocott, 1999) and keeping little or no memory of the ascent period (Paterson et al., 1998; Petford, 2003; Zák et al., 2007), although final crystallisation cannot strongly alter the preferred orientation of K-feldspar phenocrysts (Kratinová et al., 2010). Deformation partitioning in strained magmas has been rarely described for natural cases (Schulmann et al., 1997; Kratinová et al., 2007), and very little is known about the interpretation of the spatial distribution of constriction and flattening magmatic fabrics in plutons (Schulmann et al., 1997; Schulmann and Jezek, 2012). This state is partly due to the fact that no simple relationship exists between intensity and orientation of the fabric, and finite strain (Giorgis and Tikoff, 2004; Sen and Mamtani, 2006), in agreement with the outcomes of the experimental studies cited above. The third research line is devoted to the study of the rheology of granitic magmas. The first experimental data led to the proposal of rheological transitions or thresholds depending on the crystal fraction of the magma (Arzi, 1978; van der Molen and Paterson, 1979; Vigneresse et al., 1996). Granitic melt viscosities have been reasonably determined (Hess and Dingwell, 1996; Dingwell, 1999; Holtz et al., 1999; Giordano et al., 2007). Nevertheless, the scarcity of experimental rheological information on granitic magmas (however, see Rutter and Neumann (1995), Scaillet et al. (1997), Rutter et al. (2006)), and the difficulty of theoretically modelling such a complex and changing natural system, does not allow a rigorous complete understanding of this problem. Partial advances have been achieved recently, for example, with the flow of magma mushes (e.g., Koenders and Petford, 2000) or the characterisation of the parameters that control the Newtonian and Non-Newtonian rheological behaviour of granitic magmas (e.g., Caricchi et al., 2007).

In summary, despite the recent advances in the measurement and characterisation of magmatic fabrics, a more rigorous understanding of these fabrics in terms of kinematic and rheologic interpretation is still needed. A critical point is that few natural examples illustrating spatial and temporal fabric variation in granite bodies and its relations to regional strains have been analysed up to date. In this work, we present measurements of magmatic fabrics throughout three tabular granitic bodies of the Gredos massif (Variscan Spanish Central System). The results, which are well constrained by independent geochronological, geochemical and structural studies, show consistent spatial patterns that we interpret as due to the overprinting of the emplacement fabrics by those due to the tectonic regime prevalent during the formation of granitoid plutons.

2. Geological setting

The Central System batholith (e.g., Moreno-Ventas et al., 1995; Castro et al., 2002), also called Avila batholith (e.g., Bea et al., 2004a), more than 300 km in length and 60 km in width, constitutes an almost continuous granite exposure in the Central Iberian Zone of the Variscan Iberian Massif (Fig. 1a). It represents one of the largest batholiths in the Variscan belt of Western Europe. The Gredos massif, located at the centre of the Central System batholith (Fig. 1a) it is well exposed, providing a very interesting place to study the complex kinematic processes associated with the emplacement of large granitic bodies.

More than 90 vol% of the intrusive rocks of the Gredos massif is monzogranite to granodiorite composition, although minor amounts of more basic rocks ranging from quartz-diorite to gabbro also occur. Geochemically, these plutonic rocks form a typical K-rich calc-alkaline association (Capdevila et al., 1973; Moreno-Ventas et al., 1995; Díaz-Alvarado et al., 2011a). Basic rocks represent a mantle input to the source region of the granitoids and radiometric dating indicates that they are coeval or slightly earlier with respect to granodiorite generation (Bea et al., 1999). Granodiorites are coarse-grained, mesocratic rocks, commonly porphyritic (Fig. 2a, b) with large K-feldspar phenocrysts (up to 10 cm in length). They are mainly composed of Qtz, Pl (An_{32-65}), Kfs and Bt (mineral abbreviations after Kretz (1983)). Monzogranites show variable contents of Crd, particularly in areas close to the contacts with the country rocks (Díaz-Alvarado et al., 2011a). Crd-monzogranites are composed of Qtz, Pl (An_{50-32}) with complex zoning patterns, Crd and Bt. They also exhibit a porphyritic texture with large Kfs phenocrysts.

The igneous rocks in the Gredos region intruded a previously deformed host in which large extensional detachments juxtapose low-grade metasediments and anatectic complexes (e.g., Díez-Balda et al., 1995). Country rocks appear as large tabular septa, several km in length, and xenoliths to the scale of a few centimetres to hundreds of metres. The low-grade metasediments include metagreywackes and metapelites. The metagreywackes are foliated rocks, containing rounded detrital grains of Qtz, subhedral Bt, Pl and And, and anhedral Crd, Ms and Sil. These rocks were mostly transformed into migmatitic hornfelses due to the contact metamorphism associated with granite intrusion. The migmatitic hornfelses are mainly composed of phlebites and agmatites, with a paleosome formed by fine- to medium-grained metasediments and trondhjemitic to granitic leucosome veins injected parallel to the foliation of their host rocks, and also along shear surfaces and axial surfaces of minor folds affecting the layering of the paleosome. The anatectic complexes formed by low-P metamorphism and involve migmatites derived from pelitic, semi-pelitic and psammitic metasediments assigned to a several-kilometres-thick Neo-Proterozoic turbiditic series and Ordovician ferrosilicic igneous rocks similar to the Ollo de Sapo Formation (Fernández et al., 2008; Castro et al., 2009; Díaz-Alvarado et al., 2011a). Coarse-grained stromatic and nebulitic migmatites are melanocratic, heterogeneous laminated rocks, alternating with bands of felsic nebulites and schlieren of Bt. Crd–Sill–Bt-rich restites, basic enclaves of quartz-diorites and blocks of metaquartzite and phlebitic migmatites are abundant in the nebulitic migmatites. The mineral assemblage of the nebulitic migmatites is composed of Qtz with undulose extinction, subhedral Bt, Pl with normal zonation, and Kfs with perthitic textures, as well as anhedral and subhedral crystals of Crd and Sil.

The tectono-metamorphic evolution of the northern half of the Central Iberian Zone includes three main ductile deformation phases (see the relevant structural and geochronological information in e.g., Dallmeyer et al., 1997; Escuder Viruete et al., 1998; Días et al., 1998; Martínez Catalán et al., 2004; Montero et al., 2004; Bea et al., 2006; Castiñeiras et al., 2008): D1 (upright folds, contractional deformation), 360?–337 Ma; D2 (the extensional detachments), 337–320 Ma; D3 (upright folds and transcurrent shear zones), 320–300 Ma. The metamorphic peak (750 °C and 400 MPa, Pereira, 1993; Pereira and Bea, 1994) and migmatisation of the middle crust in the area occupied by the Central System batholith took place coeval with or later than the D2 phase. U–Pb and Pb–Pb

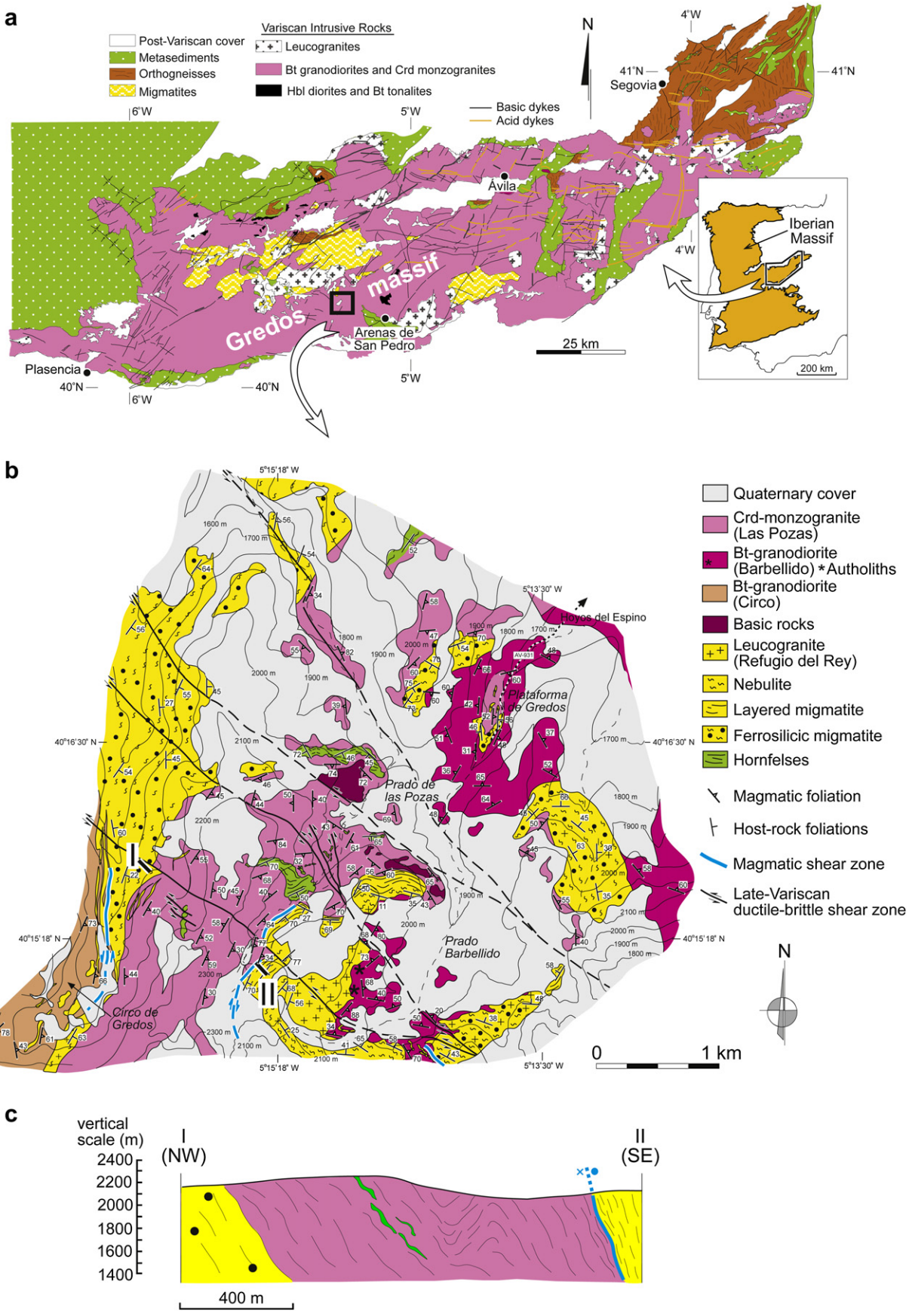

Fig. 1. Geological location of the study area. (a) Sketch of the Spanish Central System (the inset shows its location in the Variscan Iberian Massif). (b) Detailed map of the central part of the Gredos massif. (c) Cross section showing the structure of the Las Pozas Crd-monzogranite tabular body. Location in Fig. 1b. The granitic sheet was folded by the late Variscan deformation episodes, therefore increasing the apparent thickness of the originally tabular body.

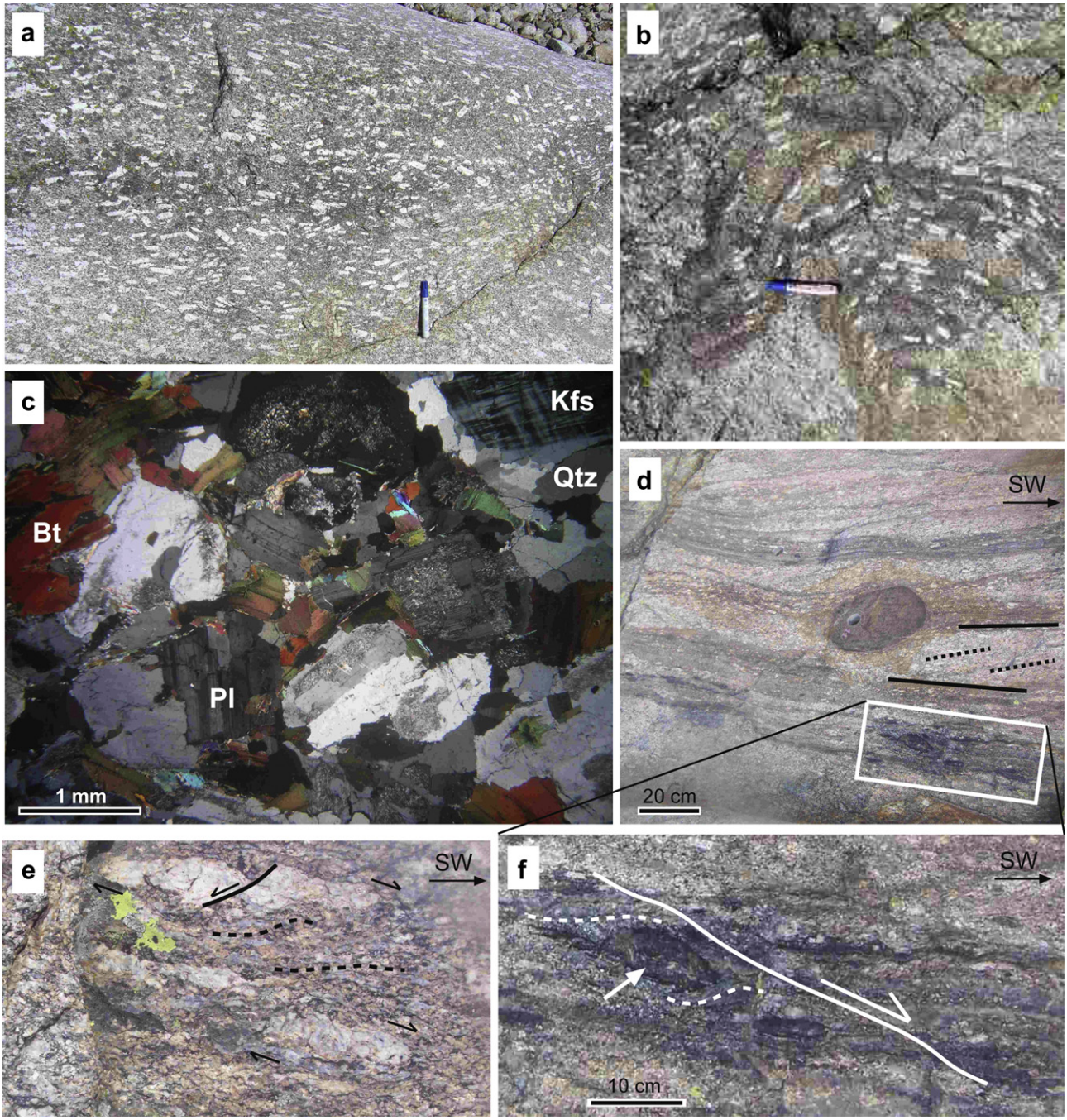

Fig. 2. Field photographs of the Gredos massif. (a) Magmatic foliation defined by the preferred orientation of the long axes of Kfs megacrysts. (b) Folded magmatic foliation. (c) Microphotograph showing the typical texture of the matrix of the granitoids. Pl and Kfs are euhedral to sub-euhedral crystals, the Pl often showing complex oscillatory zoning (large grains at the centre). Qtz occupies interstitial sites and shows scarce microstructures, mostly undulose extinction and occasional subgrain boundaries (upper right). Overall, the rocks show an igneous texture. Symbols of minerals according to Kretz (1983). (d) Magmatic and ductile shear zone at the top of Las Pozas Crd-monzogranite. Mafic enclave of rounded shape enveloped by the banding defined by schlieren, septa of migmatites, and xenoliths (black lines). The magmatic foliation defined by the preferred orientation of Kfs megacrysts (dashed black lines) is locally oblique to this banding suggesting dextral sense of shear. (e) Solid-state deformation at the base of the sheared top of Las Pozas Crd-monzogranite. σ-type Kfs porphyroclasts, some with antithetic microfaults (black line), are consistent with dextral sense of shear. (f) Close-up view of the rectangular area marked in (d). Kinematic indicators indicate dextral sense of shear: C′-type shear band (in the sense of Berthé et al. (1979); white line) and a xenolith with a geometry akin to that of σ-type porphyroclasts (white arrow).

zircon and monazite geochronology of Variscan granitoids and mafic igneous rocks of the Central System batholith and nearby regions (e.g., Días et al., 1998; Montero et al., 2004; Bea et al., 2004b; Casquet et al., 2004; Valle Aguado et al., 2005; Zeck et al., 2007) reveals that most of the Variscan magmatism is contemporary with the D3 phase. Recent U–Pb zircon geochronology for the study area showed that migmatisation of the host migmatites and hornfelses continued during the intrusion of the granitic bodies (Díaz-Alvarado et al., 2011a,b). More complete geothermobarometric analyses were possible in the Eastern

Spanish Central System, where the first stage attained up to 1400–1500 MPa and 700–800 °C, followed by an exhumation stage triggered by the D2 extensional phase, with low-pressure re-equilibration at 400–500 MPa and associated migmatisation (Castiñeiras et al., 2008). The data presented in this work cast some light on the intricacies of the D3 phase, suggesting a more complex evolution than hitherto inferred.

3. Magmatic and solid-state structures

The granitoids of the Gredos massif occur in parallel layers of variable thickness, commonly approaching 1 km (Fig. 1b, c), and extending laterally for several km. Three main granitoid bodies were mapped in the study area. The Circo Bt-granodiorite is the floor layer and its total extent is not covered by the detailed map (Fig. 1b). The Las Pozas Crd-monzogranite constitutes about 800 m thick sheet, intruded between two migmatite layers and includes several septa of migmatite hornfels, particularly near its top. The Barbellido Bt-granodiorite overlies the migmatite and related leucogranite body located at the top of Las Pozas Crd-monzogranite (Fig. 1b, c).

The granitoid layers show a variably developed magmatic foliation, mostly defined by the preferred orientation of Kfs megacrysts, and also by the parallel arrangement of enclave corridors, schlieren, xenolith septa and igneous leucocratic veins (Fig. 2). The volume fractions of Kfs megacrysts vary from less than 10% to more than 25%, with the greatest contents observed near the contacts between granitoids and host rocks. Scarce structures indicative of solid-state deformation are visible in the granitoid layers (Fig. 2c), although shear zones with predominant magmatic flow and weak ductile deformation are occasionally observed in some contacts between granitoids and migmatites (see Section 5). The whole system is pervasively invaded by several sets of leucocratic veins mostly resulting from the partial melting of the country rocks. The alternating layers of migmatites and granitoids as well as their country rock bodies are affected by at least two generations of folds, which involve a complex fold interference pattern (Fig. 3). This pattern is defined by the contacts between migmatites, granitoids and hornfels septa, as well as by the foliation inside each layer, which is mostly sub-parallel to the external contacts (Figs. 1 and 3). The axial traces of the folds of the first generation are NNE–SSW to ENE–WSW trending (Fig. 3). Folds of this generation are upright or steeply inclined, polyharmonic, with

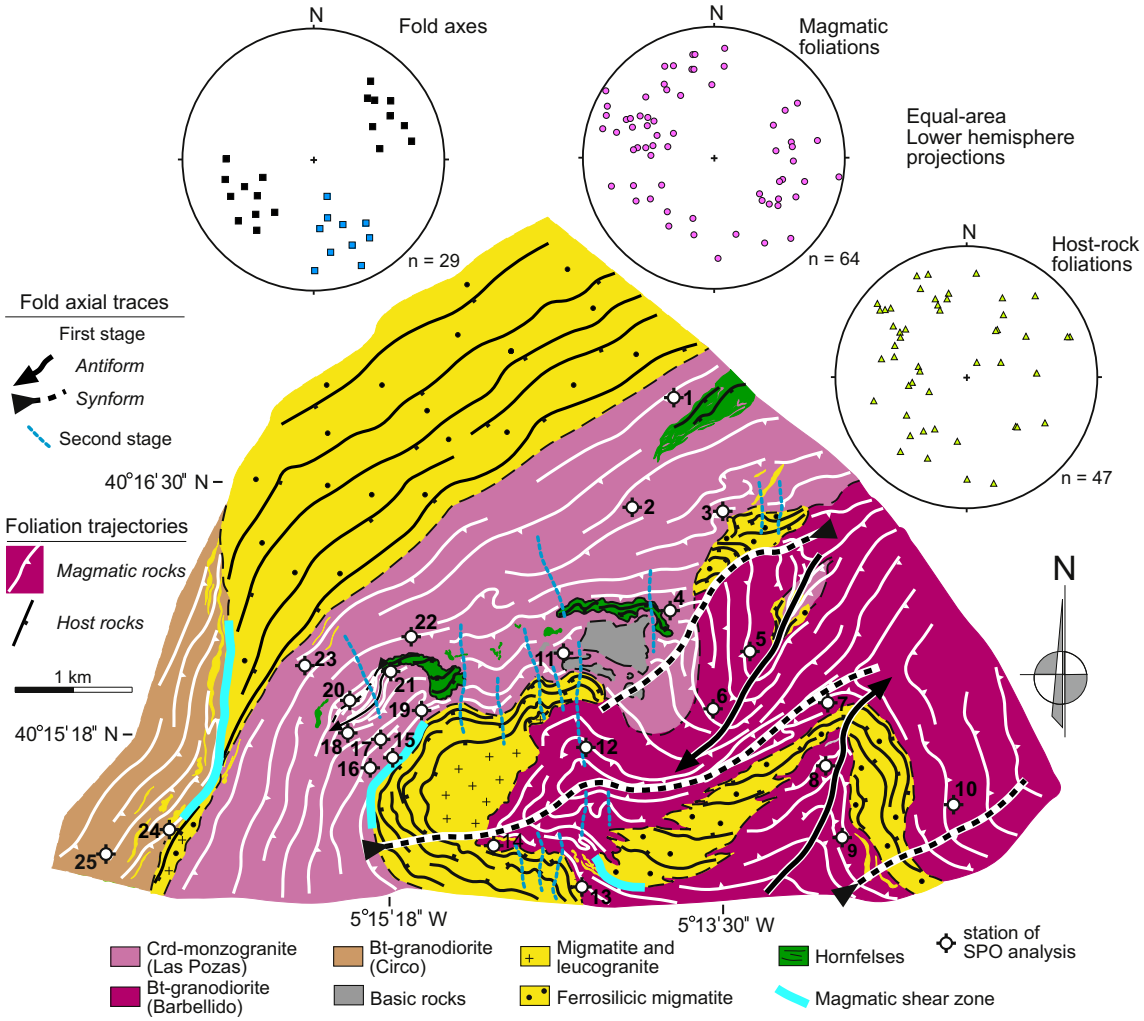

Fig. 3. Structural map of the study zone showing an interpretation after removing younger rocks and sediments and the displacements of the late ductile shear zones. Equal-area, lower hemisphere projection of fold axes (black: first generation; blue: second generation) and poles to the magmatic and host-rock foliations. (For interpretation of the references to colour in this figure legend, the reader is referred to the web version of this article.)

wavelengths ranging from less than 1 m to more than 1 km (Fig. 2b). Fold hinges are curved due to the interference with the second set of folds, and periclinal closures are frequently observed (Figs. 1b and 3). In profile, folds of the first generation are open to tight and sometimes are box folds. The axial traces of the folds of the second stage are NNW–SSE trending (Fig. 3). The fold interference pattern, although rather irregular, tends to be intermediate between types 1 and 2 of Ramsay (1967). Offsets of the fold traces are locally observed due to several late Variscan, WNW–ESE-trending, strike-slip shear zones (Fig. 1b, c). These shear zones are sub-vertical, showing decimetric to metric thickness and metric to kilometric displacement. Deformation within these shear zones is ductile–brittle, with a sub-vertical foliation and a sub-horizontal stretching lineation and slickenside striation. The abundant kinematic criteria shown by the ductile–brittle shear zones (S/C composite fabrics, asymmetric folds, extensional crenulation cleavage and many others) consistently indicate sinistral displacement. The use of these kinematic criteria together with the offset contacts enables the determination of the displacement magnitudes for the zones. Fig. 3 shows a geometric reconstruction of the mapped area after removing the displacement due to the shear zones.

4. SPO fabric of Kfs megacrysts

Kfs megacrysts are a characteristic feature in some granitic facies or suites within granodioritic to granitic components of large composite batholiths (Moore and Sisson, 2008; Farina et al., 2010). In the case of the Central System batholith, these megacrysts are present in granodiorític and monzogranitic facies (Fig. 2a), which are more than 80% vol. of the exposed batholith.

Even though the origin of Kfs megacrysts is still controversial (Vernon and Paterson, 2008; Johnson and Glazner, 2010), we infer a magmatic origin, given the euhedral habits, large sizes, or the concentric distribution of inclusions (Bt, Pl and Qtz). Additionally, in the study area, the foliation defined by the megacrysts is parallel to the main contacts between igneous and metamorphic units in the batholith, and we believe that the solid-state deformation mostly occurs in the late ductile–brittle shear zones. So, the Kfs megacryst fabric is assumed to be a magmatic fabric and Kfs megacrysts (phenocrysts) are used as suitable markers to estimate shape preferred orientation (SPO) fabrics. Magmatic foliation was measured in more than 150 sites. SPO ellipsoids were determined at 25 stations (Fig. 3). Three perpendicular field sections were analysed at each station. High-resolution digital images were taken at the studied sections and edited with Photoshop® and ImageJ editor software to extract megacrysts from the matrix, reduce image noise and to create a grey scale image file. These final images were analysed via software SPO (Robin, 2002; Launeau and Robin, 2005) to obtain the shape ratio and long axis orientation of the sectional fabric ellipses (Fig. 4a, b and c). With this information, the three-dimensional ellipsoid data were determined for each station using Ellipsoid 2003 software (Launeau and Robin, 2005). The software output includes the orientation and normalised length of each principal axis (Figs. 4d and 5c). Table 1 contains the ellipsoid data of the studied stations. Normalized standard deviations around the mean (parameter of Robin, 2002) are between 0.5 and 17% (Table 1, last data column).

To evaluate the consistency at each measurement site between the orientation of the measured magmatic foliation and that of the *XY* plane of the determined SPO ellipsoid, the dihedral angle formed by the two planes is shown in Table 1 (third column of

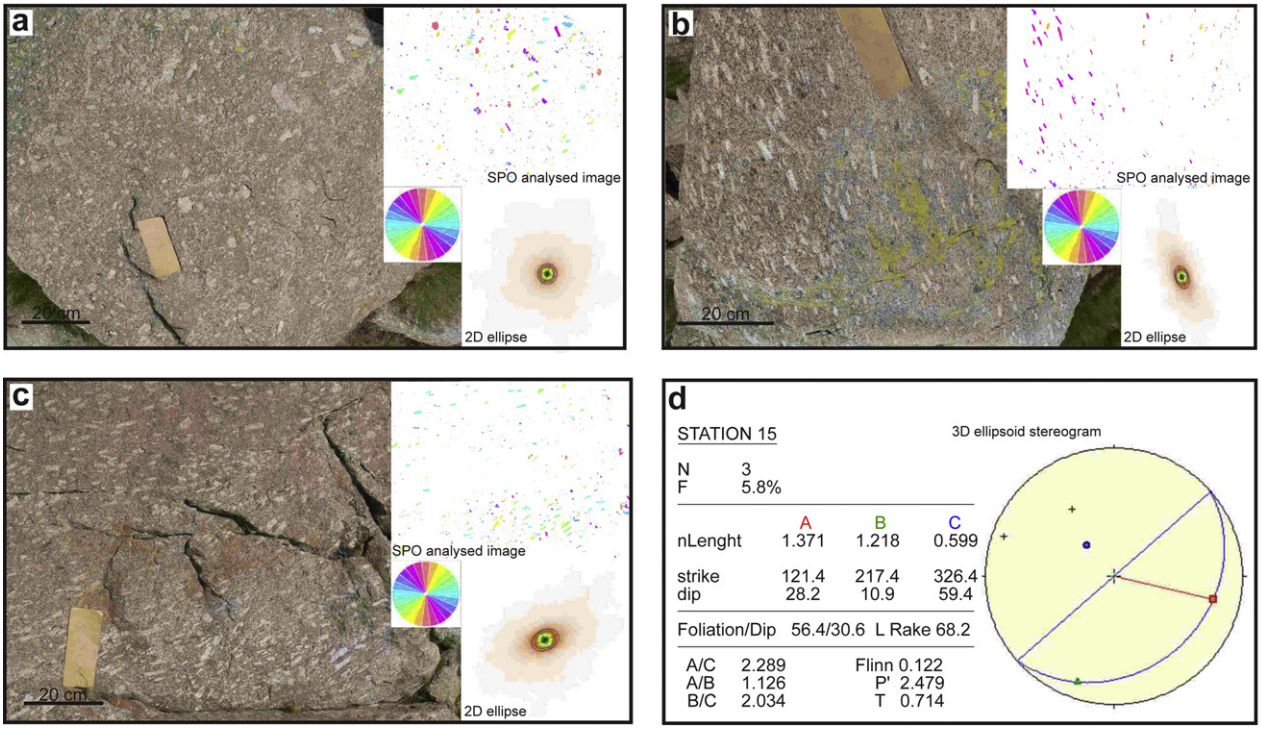

Fig. 4. Results of the SPO determination at one selected station. The fabric defined by the Kfs megacrysts was analysed from three differently oriented surfaces (a, b, c) with the SPO 2003 software (Launeau and Robin, 2005). The orientation and shape of the 3D fabric ellipsoid (d) was obtained using Ellipsoid 2003 software (Launeau and Robin, 2005).

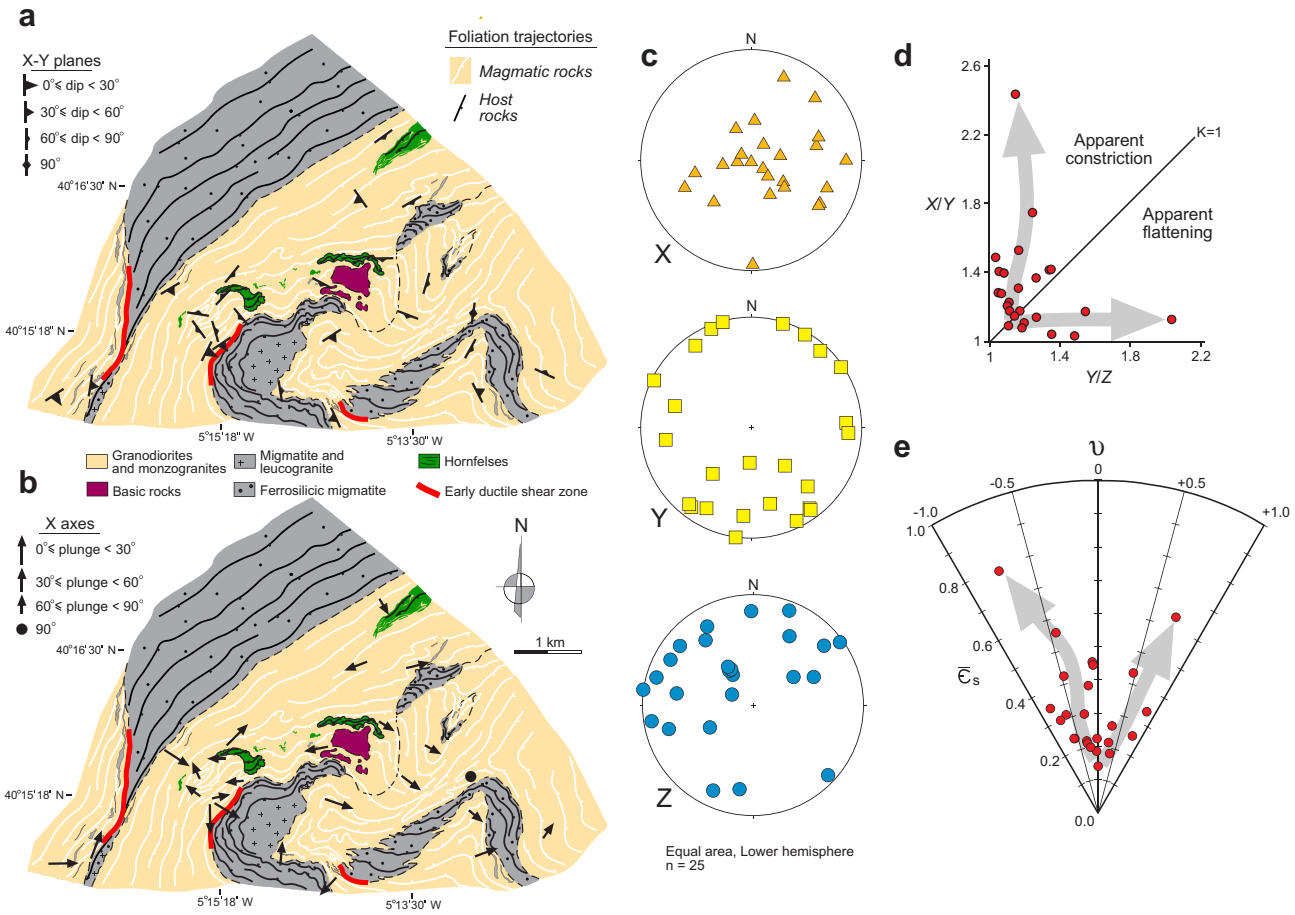

Fig. 5. Results of the SPO fabric measurement at the 25 selected sites. Plot of the orientation of the *XY* planes (a) and *X* axes (b) on a geological sketch map for the study area. (c) Spherical projection of the orientation of the *X* (top), *Y* (centre) and *Z* (bottom) axes of the SPO ellipsoid. (d) Flinn (1962) diagram showing the shape of the measured SPO ellipsoids (Table 1). (e) Hossack (1968) diagram plotting the Lode (1926, υ) and Nadai (1963, $\overline{\varepsilon}_s$) parameters (Table 1). The thick grey arrows in Fig. 5d, e show the change in the shape of the SPO ellipsoids with the increase in the fabric intensity (distance from the origin of Flinn diagram or $\overline{\varepsilon}_s$ value).

data). SPO fabrics in the flattening field show rather small dihedral angles (average value of 30° with a standard deviation of 14°), while sites with constriction fabric ellipsoids show larger dihedral angles (average value of 46° and standard deviation of 25°). The latter feature is expected from the strong inherent geometric instability of the *XY* plane in constriction ellipsoids, i.e., small variations in the original SPO data cause pronounced changes in the orientation of the *Y* axis, that is statistically poorly localized along the *YZ* plane due to the rather similar length of axes *Y* and *Z*. Apart from the effects of constrictional ellipsoids, another source of angular deviation between calculated and measured foliations is the presence of abundant xenolith and schollen bands, like those observed in stations 16 to 20, because marked variations in the orientation of foliation planes are due to the local deflection of this magmatic fabric around competent blocks. The smaller angular differences for samples with flattening fabric ellipsoids support the reliability of the technique used to determine the SPO fabric ellipsoid, and strengthen the inferences on the structural implications of the orientation and shape of the SPO fabrics at the boundaries of the granite bodies.

The greatest absolute values of the Lode's shape parameter (υ, Lode, 1926) coincide with large Nadai's intensities ($\overline{\varepsilon}_s$, Nadai, 1963) for ellipsoids both in the constriction and flattening fields (Fig. 5e, thick grey arrows, and 6), whereas most ellipsoids with shape values close to $K = 1$ ($\upsilon \approx 0$) show weaker intensities ($\overline{\varepsilon}_s \leq 0.2$). Similar relations are observed in the Flinn diagram (Fig. 5d, thick grey arrows). Isocontour maps of υ and $\overline{\varepsilon}_s$ (Fig. 6a, b) reveal that apparent flattening ellipsoids are found near granitoids contacts, so that the closer to metasedimentary bodies the greater positive values of shape parameter. Instead, ellipsoids of apparent constriction are found internally within the large granitoid bodies. Although the data are relatively sparse at fewer than 25 points, and therefore the details of the contouring should be cautiously interpreted, these results are illustrative of the general pattern. Intensity values are greater at the roof of the tabular granitoid layers. Some high intensity values for constriction ellipsoids coincide with late NNW–SSE ductile–brittle shear zones. These values might reflect this late deformation event, so these stations were not considered in the isocontour maps. These features are well illustrated in a NW–SE trending cross section (Fig. 6c, d). The post-emplacement deformation, mainly NNE–SSW folds, was eliminated at the six stations located near the cross section, to evaluate the original orientation of the ellipsoid axes inside the tabular, sub-horizontal granitoid body of Las Pozas. The restoration only considers the rotations necessary to unfold the magmatic foliation assuming that no strain affected the limbs and hinge zones of the folds. This assumption seems adequate as a first

Table 1
Data of the Kfs megacryst SPO fabric ellipsoids calculated at the 25 measurement points of the Gredos massif using Ellipsoid 2003 (Robin, 2002; Launeau and Robin, 2005).

Station	Measured foliation	Calculated foliation	Dihedral angle[a]	Ellipsoid axis[b]			Normalized axis values			Aspect ratios			Ellipsoid parameters			Normalized deviation[c] (%)
				X	*Y*	*Z*	*X*	*Y*	*Z*	*X*/*Z*	*X*/*Y*	*Y*/*Z*	Flinn	$\bar{\varepsilon}_s$ (Nadai)	υ (Lode)	
1	N40E/40SE	N54E/62SE	24°	N150E/62	N56E/2	N324E/28	1.145	0.999	0.874	1.311	1.146	1.143	1.021	0.191	−0.010	0.5
2	N148E/55SW	145E/40SW	14°	N249E/36	N154E/7	N55E/53	1.391	0.983	0.731	1.902	1.416	1.344	1.209	0.455	−0.081	12.4
3	N43E/64SE	N60E/71SE	17°	N76E/39	N220E/45	N330E/19	1.181	1.036	0.818	1.444	1.140	1.267	0.524	0.263	0.286	12.0
4	N79E/30SE	N89E/74SE	45°	N122E/62	N262E/23	N359E/16	1.335	0.974	0.769	1.735	1.370	1.266	1.391	0.391	−0.144	0.8
5	N20E/20NW	N16E/80SE	79°	N119E/80	N17E/2	N286E/10	1.397	0.914	0.783	1.783	1.529	1.167	3.168	0.424	−0.467	11.6
6	N168E/55SW	N111E/81SW	59°	N127E/59	N286E/29	N21E/9	1.897	0.778	0.677	2.801	2.437	1.15	9.580	0.790	−0.729	2.7
7	N70E/52NW	N8E/90	68°	N96E/90	N188E/0	N278E/0	1.202	0.940	0.885	1.358	1.278	1.062	4.484	0.229	−0.604	10.0
8	N26E/37NW	N29E/74SE	72°	N130E/74	N30E/3	N299E/16	1.203	0.936	0.888	1.355	1.285	1.054	5.278	0.230	−0.652	3.3
9	N147E/55NE	N153E/36E	20°	N70E/35	N338E/4	N243E/54	1.389	0.982	0.733	1.896	1.414	1.340	1.218	0.453	−0.084	4.8
10	N143E/48NE	N115E/74E	35°	N35E/74	N296E/3	N205E/16	1.139	1.025	0.856	1.332	1.111	1.198	0.561	0.205	0.263	11.0
11	N130E/65SW	N118E/60SW	12°	N259E/47	N136E/27	N28E/30	1.281	0.919	0.850	1.507	1.393	1.081	4.852	0.308	−0.618	8.0
12	N4E/48SE	N57E/34SE	37°	N109E/28	N209E/18	N327E/56	1.261	0.961	0.825	1.528	1.311	1.165	1.885	0.304	−0.278	4.4
13	N139E/42NE	N155E/51SW	88°	N223E/49	N326E/11	N65E/39	1.183	0.970	0.872	1.357	1.22	1.112	1.964	0.219	−0.303	2.3
14	N12E/90	N171E/82NE	22°	N5E/59	N166E/30	N261E/8	1.172	0.970	0.880	1.332	1.207	1.103	2.010	0.206	−0.315	12.9
15	N42E/63SE	N56E/31SE	33°	N121E/28	N217E/11	N326E/59	1.371	1.218	0.599	2.289	1.126	2.034	0.122	0.633	0.714	5.8
16	N26E/30SE	N27E/17SE	13°	N179E/8	N87E/15	N297E/73	1.158	0.981	0.880	1.315	1.180	1.115	1.565	0.195	−0.207	17.0
17	N34E/59SE	N164E/68NE	46°	N78E/68	N345E/1	N254E/22	1.114	1.031	0.870	1.281	1.081	1.185	0.438	0.179	0.374	5.7
18	N20E/73SE	N144E/87SW	58°	N307E/81	N144E/9	N54E/3	1.317	0.886	0.857	1.537	1.487	1.034	14.324	0.338	−0.846	2.0
19	N48E/64SE	N140E/73SW	45°	N265E/69	N144E/11	N50E/17	1.277	0.909	0.861	1.482	1.404	1.056	7.214	0.301	−0.724	7.0
20	N174E/57NE	N99E/66NE	66°	N336E/63	N93E/13	N189E/24	1.175	0.999	0.852	1.379	1.176	1.173	1.017	0.227	−0.009	14.6
21	N82E/41NW	N43E/82NW	52°	N270E/80	N42E/7	N133E/8	1.559	0.893	0.718	2.172	1.746	1.244	3.057	0.566	−0.437	0.4
22	N18E/24SE	N39E/74SE	52°	N45E/19	N182E/64	N309E/16	1.137	1.091	0.806	1.41	1.042	1.353	0.119	0.265	0.759	10.6
23	N26E/28SE	N59E/31SE	15°	N123E/28	N219E/12	N329E/59	1.099	1.001	0.909	1.210	1.098	1.102	0.961	0.135	0.022	6.2
24	N25E/44SE	N9E/59SE	19°	N21E/19	N138E/52	N279E/31	1.162	1.129	0.762	1.526	1.029	1.482	0.060	0.334	0.863	12.9
25	N35E/47SE	N57E/27SE	24°	N89E/15	N185E/21	N327/63	1.284	1.097	0.710	1.807	1.170	1.544	0.313	0.433	0.468	13.4

[a] Dihedral angle between measured and calculated foliation.
[b] Trend/Plunge.
[c] Parameter $\sqrt{\bar{F}}$ of Robin (2002).

approximation, because no systematic variation of the SPO fabric is associated with the geometric elements of the mapped folds (compare Figs. 3 and 6a, b). Fig. 6e shows the attitude of the principal axes of the SPO ellipsoid before (left stereogram) and after (*X*, *Y* and *Z* restored stereograms) this restoration process. The *X* and *Y* axes are located along major circles in their inferred old attitude, whereas most of the restored *Z* axes are sub-vertical.

5. The sheared top of the Las Pozas Crd-monzogranite

The top of the Las Pozas monzogranite in contact with its migmatitic host rock is affected by a sub-parallel shear zone about 15 m thick (Figs. 1 and 2d). Similar shear zones occur at the top of the Circo and Barbellido Bt-granodiorites. The structural characteristics of these three sheared contacts between granitoids and host rocks are virtually identical, including the presence of parallel-sided zones, several metres thick, with alternating bands of granitoid and host migmatite. The granitoid bands show prominent magmatic fabrics, although all the sheared contacts contain minor, discrete shear bands, with evidences of solid-state deformation. The three shear zones show compatible kinematic characteristics and evolutions. In particular, kinematic criteria are consistent for the magmatic and solid-state deformations at each sheared contact. Therefore we have focused on the analysis of the well-exposed sheared top of the Las Pozas sheet, which is considered illustrative of the entire structural evolution of the massif. A detailed description of this shear zone in terms of outcrop-scale structure, kinematic indicators and evidence of deformation relative to intrusion is relevant to understanding the mechanisms that operated in the Gredos massif to generate the observed magmatic fabrics.

5.1. Structure

The average orientation of the shear zone is N45°E, dipping around 60°SE (Fig. 1). The shear zone is characterised by the presence of alternating bands, 5–30 cm thick, composed of Crd-monzogranite and migmatite, and arranged parallel to the boundaries of the zone (Fig. 2d). The banding is interpreted to have formed by successive intrusion of sill-like bodies of granitoid magma inside the migmatitic host rocks, at the boundary of the main magma batch of Las Pozas with stretching of the alternating bodies (magma and host-rock septa) within the shear zone (Díaz Alvarado et al., 2006, 2007). The lineation defined by the preferred orientation of the Kfs megacrysts is sub-horizontal. The foliation observed inside the Crd-monzogranite bands, marked by the strong preferred orientation of the Kfs megacrysts in the Crd-monzogranite, is locally oblique to the lithological banding (Fig. 2d), consistently indicating a dextral shear sense. Other kinematic indicators of dextral displacement are best seen on surfaces normal to the foliation and parallel to the lineation. These indicators include C′-type shear bands (Fig. 2d, f) and restite blocks or mafic enclaves with asymmetrically arranged, adjacent host foliations (Fig. 2f), yielding geometries akin to σ-type and δ-type mantled porphyroclasts (Passchier and Trouw, 1996). The study of thin sections revealed that deformation occurred in the magmatic state, due to the absence of microstructures indicating plastic deformation in the minerals constituting the Crd-monzogranite. However, some evidences of solid-state deformation can be observed at the base of the shear zone, where Crd-monzogranite bands contain stretched Qtz grains (Fig. 2e), defining a foliation oblique to the borders of the bands. Other structures due to solid-state deformation are stepped fragments of Kfs crystals due to microfaulting and σ-type

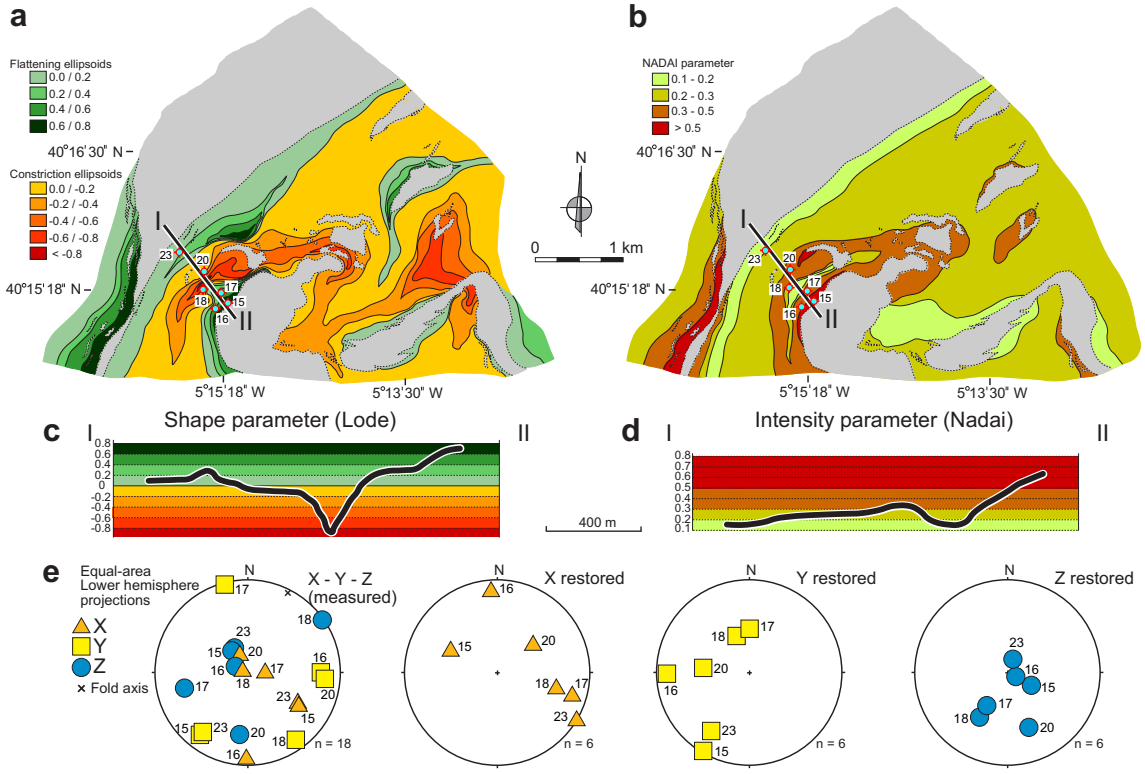

Fig. 6. Spatial distribution of (a) the shape (Lode's parameter) and (b) intensity (Nadai's parameter) of the SPO fabric ellipsoid for Kfs megacrysts. Isocontours were traced using the kriging contouring method. (c) and (d) show the variation across cross section I–II (see Fig. 1c) of the Lode's and Nadai's parameters, respectively. (e) Projection of the *X*, *Y* and *Z* principal axes of the SPO fabric ellipsoids found at 6 measurement places (15, 16, 17, 18, 20, 23, see Table 1) near cross section I–II. Left diagram: Present-day attitude of the principal axes. Remaining diagrams: Restored orientation of the *X*, *Y* and *Z* axes after eliminating the late folding episode. The primitive coincides with the boundaries of the granitoid body at the diagrams with the restored position of the principal axes of the SPO ellipsoid.

Kfs porphyroclasts (Fig. 2e). All these kinematic criteria show dextral sense of shear for the solid-state deformed band of the shear zone. No similar ductile shear zones are found in the granitoid sheets outside their sheared tops, apart from the late Variscan, sub-vertical, brittle–ductile shear zones. Given the spatial association between the magmatic and solid-state shear zones, and their consistent kinematics, a continuous transition from magmatic to solid-state flow is inferred.

In summary, we infer a predominantly dextral strike-slip shear sense for the present-day attitude of the sheared top of the Las Pozas Crd-monzogranite sheet. Onset of shearing occurred at the magmatic state and continued during solid-state deformation at the sheet base after complete crystallisation of the Crd-monzogranite.

5.2. Interaction between Kfs megacrysts

Magmatic tiling, defined as the interaction between early-formed crystals, oriented mutually sub-parallel, that translate and rotate within a viscous melt due to magmatic flow and/or deformation, can be used as a kinematic indicator (e.g., Mulchrone et al., 2005 and references therein). As a result, tiling can be used to deduce kinematically the sense of shear of magmatic flow or deformation imposed on magmatic media (e.g., Blumenfeld and Bouchez, 1988). However, a relatively large proportion of tiling particles will show the opposing sense of shear relative to the overall flow, which has led different authors to consider magmatic tiling as not a reliable sense of shear criterion (e.g., Passchier and Trouw, 1996). To avoid this problem, Mulchrone et al. (2005) suggest analysing a minimum of 50 tiling megacrysts to generate a consistent sense of shear. In addition to shear-sense determination, it has been recently proposed (Mulchrone et al., 2005) that magmatic tiling can be used also as a kinematic vorticity gauge, although a minimum of 200 tiling megacrysts should be analysed to produce reliable results.

In this work, a methodology for the analysis of interacting megacrysts (i.e., tiling and non-parallel interactions) that expands the approach originally proposed by Mulchrone et al. (2005) was applied (Appendix 1). One sample located at the shear zone at the top of the Las Pozas Crd-monzogranite (close to measurement site 15, Fig. 3) was analysed. The section is approximately orthogonal to the foliation defined by the megacrysts and parallel to the lineation marked by their preferred alignment (Fig. 7). All interaction groups identified in the sample (501) were analysed, which implies the inspection of a minimum of 1002 individual Kfs megacrysts. 138 groups produced ambiguous sense of interaction, because of mutually inconsistent senses within pairs and/or because distinct senses of interaction deduced from pairs of the same group. This gives a total number of 363 consistent senses of interaction. From these, 213 (59%) were dextral and 150 (41%) were sinistral. The results are shown in Table 2. Consequently, deduced shear sense is dextral.

The confidence interval (M_U–M_L, see Eq. (A2), Appendix 1) for the sample is 0.1, and the number of analysed groups is larger than 200, which are within the range of acceptable values (Mulchrone et al., 2005) for obtaining reliable kinematic vorticity estimations (see also Appendix 1). The crystal fraction, given as the proportion

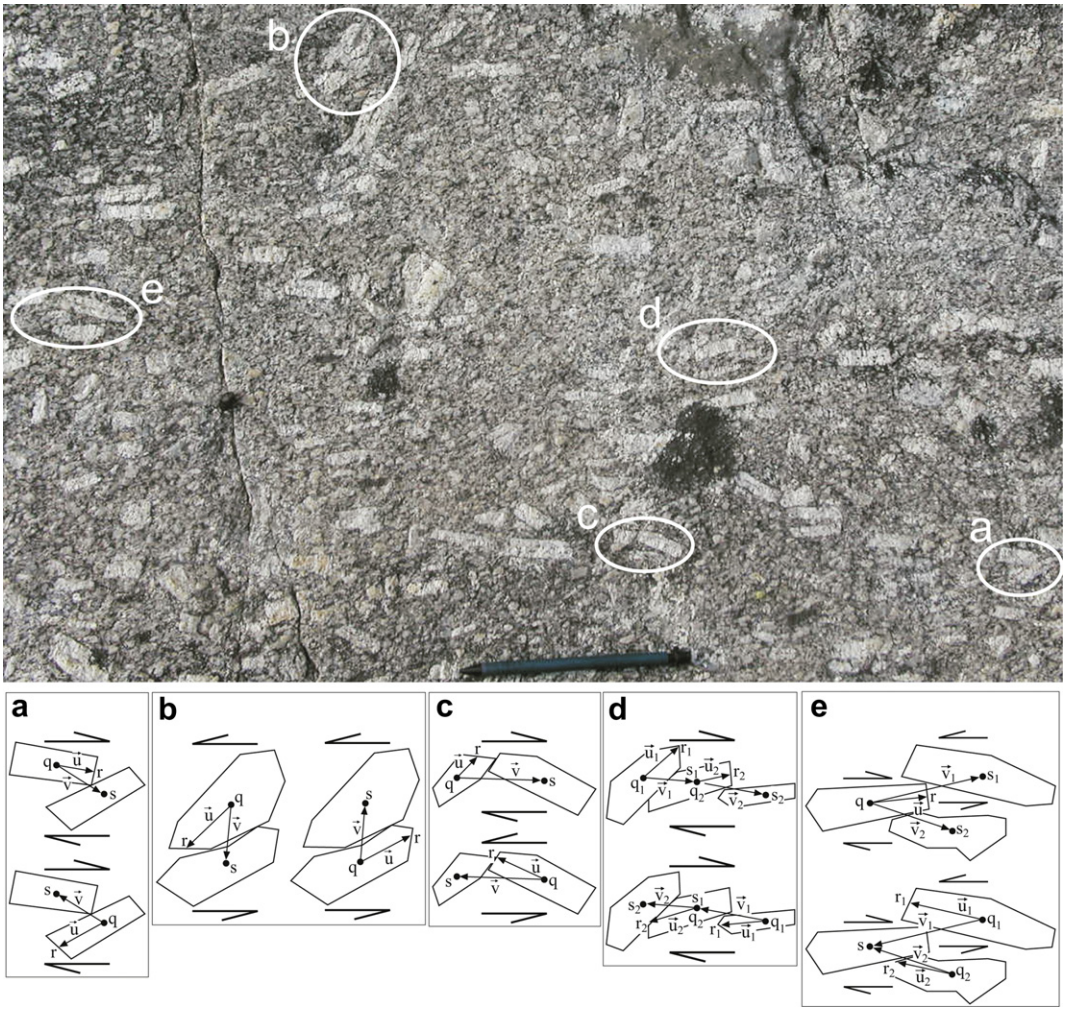

Fig. 7. Field examples illustrating determination of the rotation sense from interacting groups of Kfs megacrysts. (a) Dextral pair. (b) Sinistral pair (note antithetical geometry). (c) Inconsistent pair. (d) Unambiguous dextral group. (e) Ambiguous group. From these, only groups (a), (b) and (d) should be used to deduce the sense of shear and kinematic vorticity.

of the area occupied by the entire megacryst population to the total sampled area, is ~15%, which is within the range of the estimated fraction of Kfs megacrysts across the studied area at around 10–25%, and the average aspect ratio of megacrysts is $R \approx 2$. With these parameters, the resulting spacing is ~200 (see Eq. (A3)). According to Mulchrone et al. (2005), values of spacing larger than 110 are far below the rheological critical melt percentage (Arzi, 1978). Therefore, rigid-body rotation of megacrysts included in a viscous magma with Newtonian behaviour can be assumed in this case (e.g., Vigneresse et al., 1996). The results were compared with theoretical predictions of tiling with a spacing of 200 and an average aspect ratio (R) of 3 (Mulchrone et al., 2005), even though the sample has an average R of 2, although this difference in R does not significantly affect the comparison (Mulchrone et al., 2005). The

Table 2
Results of the analysis of sense of rotation deduced from the interacting groups in the granite deformed by the Las Pozas shear zone (see Appendix 1 for an explanation of the parameters in the table).

n	Dextral (M)	Sinistral	M_L	M_U	M_U–M_L	W_{kL}	W_k	W_{kU}
363	0.59	0.41	0.53	0.63	0.1	0.81	0.85	1.03

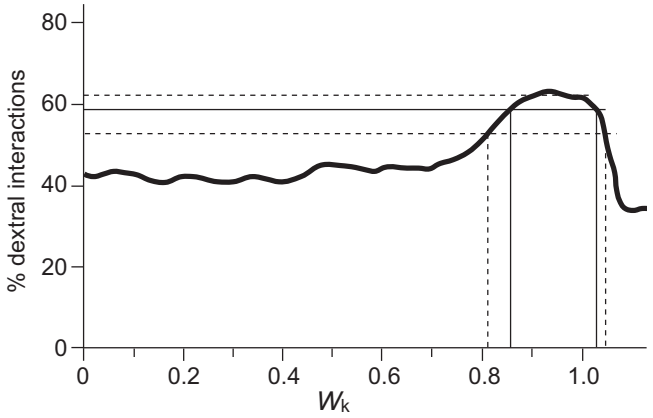

Fig. 8. Relation between proportion of interactions with dextral sense and kinematic vorticity W_k (thin solid line). The thick line corresponds to the proportion of dextral tiling pairs mathematically predicted for aspect ratio $R = 3$ and spacing $p = 200$ (from Fig. 14c of Mulchrone et al. (2005)). Dashed lines represent lower and upper limits for dextral interactions (confidence interval) and their respective W_k values (see also Table 2).

lower limit of dextral interactions ($M_L = 0.53$) would correspond to a kinematic vorticity of $W_k = 0.81$, whilst the upper limit ($M_U = 0.63$) would match with a kinematic vorticity of $W_k = 1.03$ (Fig. 8). The central value ($M = 0.59$) gives a kinematic vorticity of $W_k = 0.85$ (Table 2). Therefore, the analysis of interacting megacrysts in the granite affected by the Las Pozas shear zone suggests that this shear zone was affected by a dextral simple-shearing component accompanied by a pure-shearing component yielding a kinematic vorticity of around 0.85.

5.3. Quartz lattice preferred orientation

Two samples were used to analyse the quartz lattice preferred orientation. Both are located at the sheared top of the Las Pozas Crd-monzogranite (site 15, Fig. 3). One sample is a quartzite layer within the stromatic migmatites affected by the shear zone. Quartz grain size ranges from 1 to 20 mm in diameter. Microstructures include undulose and chess-board extinction, lobulated and serrated grain boundaries, "island grains", subgrain boundaries and polygonal aggregates. We interpret the formative deformation processes to be grain-boundary migration and subgrain-rotation dynamic recrystallization (Díaz-Alvarado et al., 2007 and references therein). The other sample corresponds to a Crd-monzogranite deformed in the solid state inside the same shear zone. Elongate quartz crystals (1–2 mm length) present undulose and chess-board extinction, lobulated grain boundaries and mosaics of fine-grained (≤0.1 mm) dynamically recrystallized grains. Mica crystals are often bent and kinked, affected by dynamical recrystallization and elongate, defining with the quartz grains an incipient mylonitic foliation. Micas fishes are common. Feldspar crystals (Kfs and Pl) are large (2–4 mm in the matrix and megacrysts of >10 mm) and show abundant undulose extinction, some mechanical twins and abundant microfractures. Kinematic criteria (mica fishes, foliation oblique to the shear boundary) consistently indicate dextral displacement.

Quartz lattice preferred orientation was determined via electron backscattered diffraction (EBSD) in scanning electron microscope (SEM). The quartzite sample was analysed in a Philips XL-30 at the CITIUS (University of Seville, Spain), operating at 20 kV accelerating voltage and a working distance of 10 mm. The Crd-monzogranite was analysed at the CIC (University of Granada, Spain), in a Gemini-1530 of Carl Zeiss operating at 15 kV and a working distance of 12 mm. Both samples were prepared via mechanical and chemical polishing, followed by thin carbon coating. EBSD patterns were indexed and processed to obtain pole figures by software OIM-analysis v.3.5 of TSL.

The measured quartz *c*-axis fabrics show a main maximum located close to the pole of the foliation, slightly deviated in a clockwise sense from it (Fig. 9). A secondary maximum is located near the *X* direction. An additional secondary maximum close to the *Y* direction is observed in the quartzite sample whereas the Crd-monzogranite sample presents a vague girdle passing through the *Y* direction and oblique to the foliation plane. The shape of the observed Qtz *c*-axis fabrics (Fig. 9) suggests a rotational component with a dextral sense of shear. The absence of clear asymmetric crossed girdles can be attributed to dynamic recrystallisation (Jessell, 1988) and/or to the contribution of a non-rotational component during deformation (Lister and Hobbs, 1980; Schmid and Casey, 1986), which would correspond, in this case, to sub-vertical shortening, i.e. orthogonal to the original attitude of migmatitic layering (Díaz-Alvarado et al., 2007).

In summary, the results of the study of magmatic tiling and of quartz *c*-axis fabrics, although scarce, are considered representative of the analysed structure, because they are consistent with the other kinematic criteria indicating a dextral sense of displacement for the sheared top of Las Pozas magmatic body. After restoring the effects of the late folding, we infer that the shear zone was sub-horizontal and the restored shear-sense is top-to-the-SW. Our results are consistent with deformation involving a combination of simple and pure shearing in a sheared top to the granitic body, because of vorticity values of around 0.85 determined from the analysis of interaction between Kfs megacrysts, quartz *c*-axis fabric data with a strong maximum close to the pole of the foliation, and flattening SPO fabric ellipsoids.

6. Discussion

6.1. Kinematic interpretation of the emplacement and shearing of the studied granitoids

Kfs SPO fabrics of the Gredos massif are potentially a powerful tool to infer emplacement mechanisms and coeval regional

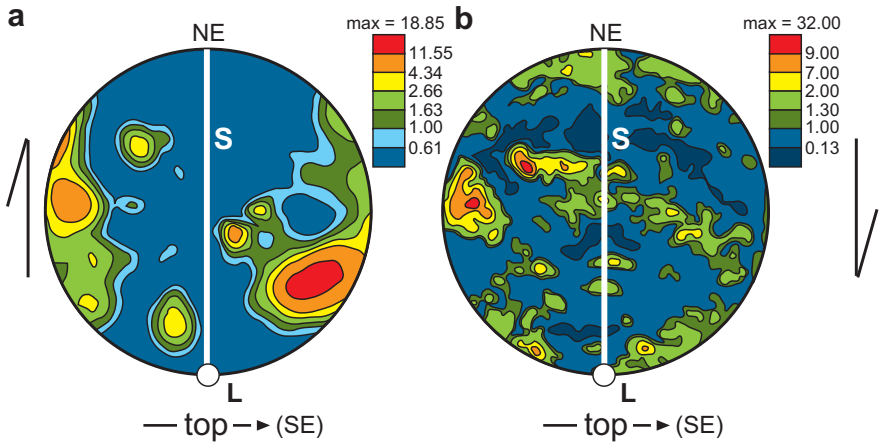

Fig. 9. Quartz *c*-axis fabrics measured by SEM/EBSD from two samples from the shear zone at the top of the Las Pozas Crd-monzogranite body (measurement site 15, Fig. 3). Lower-hemisphere, equal area projections. Contour intervals are multiples of uniform distribution (mud). S: foliation plane; L: lineation. (a) Qtz-rich level inside a migmatite band (b) Crd-monzogranite deformed in the solid state.

tectonics. Our analysis does not focus on the spatial variation in ellipsoid shapes as a function of finite strain (Giorgis and Tikoff, 2004; Sen and Mamtani, 2006), because such a relationship is complicated by the process of acquisition of SPO fabrics for rotating rigid crystals under distinct flow types (e.g., Fernandez and Fernández-Catuxo, 1997; Arbaret et al., 2000; Jiang, 2007), and the issue of diachronous and heterogeneous evolution of magmatic fabrics during and after emplacement, cooling and even reheating of distinct magmatic units along active tectonic structures (Zák et al., 2007, 2008; Kratinová et al., 2007).

In the Gredos massif, magmatic and solid-state foliations measured in more than 100 sites reveal a structural continuity between the metasedimentary host and granitic bodies during, at least, the post-emplacement folding stages (Figs. 3 and 5). The same applies to the measured Kfs SPO fabrics (Fig. 6). Geometrical and kinematic identity between the magmatic and solid-state structures and fabrics analysed at the sheared top of the Las Pozas Crd-monzogranite (Section 5) further strengthen this argument. Continuity between the magmatic fabrics in the granitoid bodies and the country-rock structures suggests that all fabric patterns were probably strongly influenced by regional deformation during D3 Variscan deformation phase, consistent with interpretations from other igneous bodies (Paterson et al., 1998; Benn et al., 2001; Sen and Mamtani, 2006; Kratinová et al., 2007).

Two distinct types of SPO fabrics were observed (Figs. 5 and 6): Near the contacts with the metasedimentary host rocks, fabrics suggest apparent flattening; whereas the inner zone of the granite bodies are characterised by constriction SPO fabric ellipsoids. Schulmann et al. (1997) described a very similar pattern measured along *ca*. 1 km of a borehole drilled across a porphyritic granite. Given a lack of a consistent relation between the fabric symmetry and the two generations of D3 folds we infer that this fabric pattern was acquired prior to D3 folding, during the syn-tectonic emplacement and deformation of the granitoid bodies.

The characteristics of the SPO fabric at the boundaries of the granitic bodies are consistent with data from Qtz *c*-axis fabrics and interaction between Kfs megacrysts. SPO ellipsoids are in the apparent flattening field (Fig. 5), the fabric intensity increases towards the top contact (Fig. 6b, d), and the average kinematic vorticity is 0.85, consistent with almost equal dextral simple-shearing and pure-shearing dominated flow (e.g., 0.81, Fossen and Tikoff, 1998). Flattening and even oblate ellipsoids are expected for this kinematic vorticity after moderate to intense finite strains (e.g., Fernández and Díaz-Azpiroz, 2009). Thus, we infer that the SPO fabrics at that body boundaries are the result of the general fabric formed during emplacement overprinted by dextral shearing with pure shearing during subsequent deformation between the body and the host rock.

According to these data and interpretations, a simple model of fabric acquisition and partitioning is proposed (Fig. 10). The structures are interpreted as evidence that the pluton fabric was mostly induced by regional deformation. Syntectonic emplacement of granitic magmas along D3 subhorizontal extensional shear zones (Fig. 10a) induced an essentially constrictional magmatic fabric in plutons. This pattern is present in a number of Variscan plutons and the explanations for these constrictional fabrics include overprinting of a slightly constrictional flow on previous fabrics, probably related to magma ascent and emplacement (Kratinová et al., 2012). Late during pluton emplacement and deformation (Fig. 10b), flow became localised along the roof of the intruded granitic sheets. Overprinting of the previous fabric by sub-horizontal simple shearing and coeval sub-

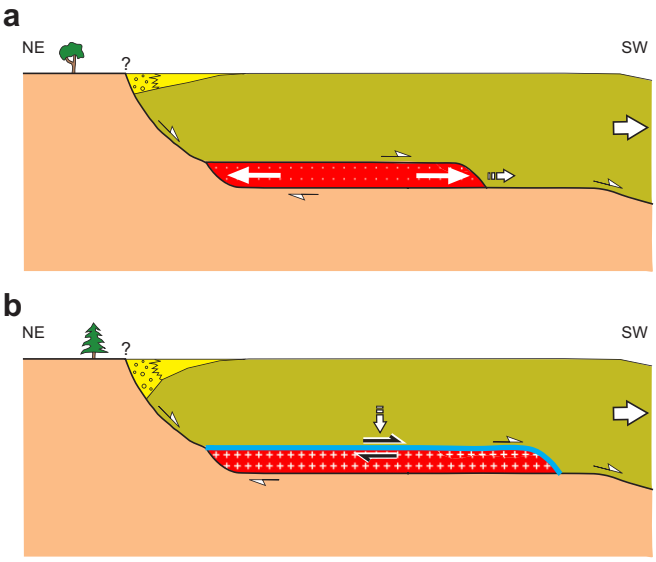

Fig. 10. Conceptual model of emplacement of magma batches at extensional detachments. (a) First stage: growth of the pluton as a sub-horizontal sheet complex exploiting an extensional detachment, possibly at a dilation jog, releasing bend or similar structure. (b) Second stage: Reworking of the roof of the pluton as a consequence of simple shearing (thick blue line) and, possibly, flattening due to the extensional collapse of the crust (vertical arrow) and/or gravity ascent of magma inside the pluton. (For interpretation of the references to colour in this figure legend, the reader is referred to the web version of this article.)

vertical shortening within the bounding shear zones yielded the intense flattening fabrics of pluton roofs. This kinematic behaviour is similar to transpression (e.g., Schulmann and Jezek, 2012; Kratinová et al., 2012 and references therein). The deformation of pluton roofs continued after their complete crystallisation. This model of syn-tectonic emplacement and deformation of granitoid magmas at the Gredos massif can be used to clarify some points about the late episodes of structural evolution of this part of the Variscan Belt.

6.2. Structural evolution

The Variscan deformation of the study region started with the D1 contractional phase, followed by D2 extensional detachments. At the end of this extensional period (≈320 Ma), low-grade metamorphic rocks became tectonically juxtaposed onto high-grade domains (Fig. 11a). The structures of the D1 and D2 Variscan deformation phases are crosscut by the granitoids at the northern boundary of the Central System batholith (e.g., Doblas, 1991; Fernández and Castro, 1999), which agrees with the geochronological data. The D2 phase was followed by a period (≈320–300 Ma) of strongly heterogeneous and complex deformation (e.g., Martínez Catalán et al., 2009), which is collectively assigned to the D3 deformation phase. D3 began with an extensional phase (Fig. 11b), coincident with the period of late-orogenic collapse identified in other regions of the Variscan Orogenic Belt like the French Massif Central (Faure, 1995; Talbot et al., 2005; Joly et al., 2009). Granites intruded coevally with this extensional episode of the D3 deformation phase (Fig. 11). The emplacement of the granodiorites and monzogranites of the Gredos massif occurred at rather shallow depths (ca. 400 MPa; Pereira, 1993; Pereira and Bea, 1994; Castiñeiras et al., 2008), considering the large thickness estimated for the Variscan crust in this area (Villaseca et al., 1999). At the intrusion level, the granitoid magma

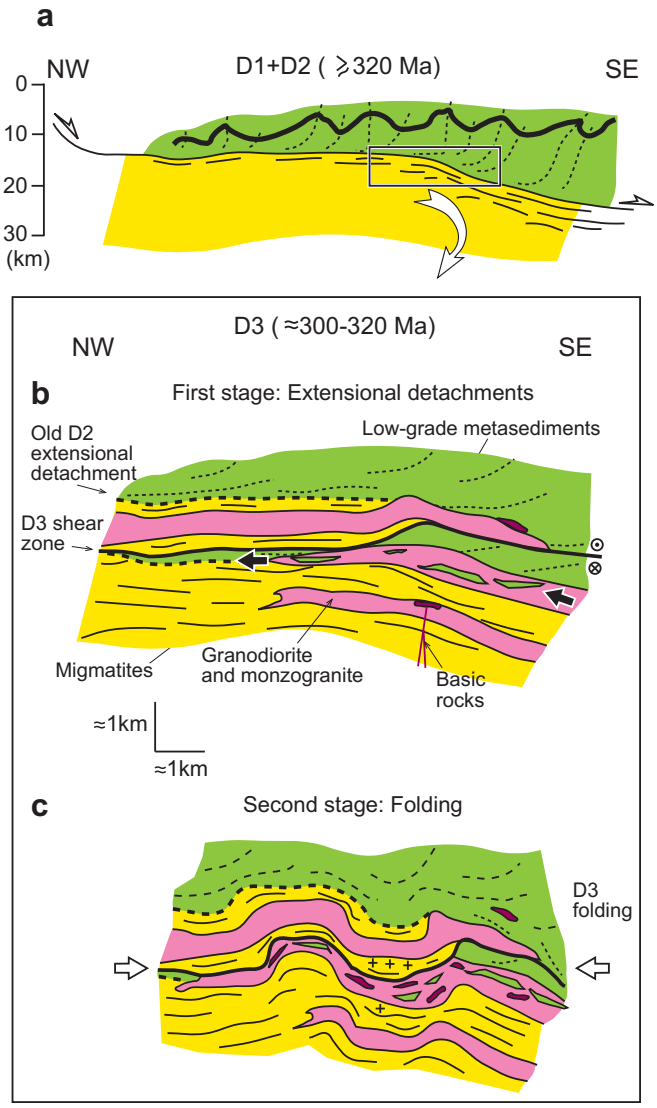

Fig. 11. Evolution model of the Spanish Central batholith. (a) Schematic cross section of the central part of the Spanish Central System during extensional detachments characteristic of the Variscan second deformation phase (D2). Low-grade metamorphic rocks (green) were tectonically juxtaposed above high-grade domains (yellow), which became partially molten creating a mid-crustal migmatitic belt. The hangingwall (green) shows D1 folds reoriented by the D2 extensional detachments. The rectangle indicates the approximate location of the area enlarged in (b) and (c). (b) Initial D3, with ductile extensional structures (bold black lines) and sequential emplacement of granitoid batches (pink). (c) Later D3 deformation with two generations of upright folds and ductile–brittle, sub-vertical, discrete shear zones (not shown) that deformed the entire system. (For interpretation of the references to colour in this figure legend, the reader is referred to the web version of this article.)

became variably contaminated with the host rocks (Díaz-Alvarado et al., 2011a). In the study area, the successive magma batches intruded sequentially along a rather prolonged time period spanning near 10 Ma, from 312 to 303 Ma (Díaz-Alvarado et al., 2011b). The D3 extensional episode was followed by the generation of upright folds (Fig. 11c). Similar complex structural evolutions have been described elsewhere for the D3 phase at the Central Iberian zone (Días et al., 1998; Escuder Viruete et al., 1994; Valle Aguado et al., 2005). In particular, our structural history and behaviour is analogous to behaviour during the oroclinal bending of the Ibero-Armorican Arc that took place at about 295–310 Ma according to Weil et al. (2010), Gutiérrez-Alonso et al. (2011) and Pastor-Galán et al. (2011).

7. Conclusions

A detailed mapping and structural study of the granitoid bodies of the central region of the Gredos massif (Spanish Central System batholith) reveals that the igneous rocks are tabular-like bodies intruded into a predominantly migmatitic country-rock during the first extensional stage of the D3 deformation phase of the Variscan Orogeny. The magmatic intrusions exploited large-scale, sub-horizontal, extensional shear zones. Kfs SPO ellipsoids are in the constriction field at the centre of the distinct granitic septa, which is a consequence of the overprinting of slightly constrictional flow on previous emplacement fabrics during the growth of the laminar plutons along releasing bends or similar structures associated with D3 extensional detachments. Additionally, Kfs SPO ellipsoids measured at the margins of the granitic bodies, affected by shear zones evolving from the magmatic to the solid-state, are in the apparent flattening field, and their short axes are oriented nearly normal to these margins. Kinematic analysis yielded a kinematic vorticity number of around 0.85, which we infer to result from a combination of vertical shortening, probably due to the extensional collapse of the crust or to the gravity-driven ascent of magma, with tectonic dextral simple shearing along the shear zones. Finally, the last stages of the Variscan D3 phase repeatedly folded the previous structures, creating their present-day geometry.

Acknowledgments

This work is part of the PhD Thesis of J.D.A., carried out at the Departments of Geology and Geodynamics and Palaeontology, University of Huelva., with a Grant Fellowship from the Spanish Ministry of Science and Innovation (Grant No. AP2005-3498). The work was funded with Projects CGL2004-06808-CO4-01/BTE, CGL2004-06808-CO4-02/BTE, CGL2007-63237/BTE, and CGL2010-22022-CO2-01 of the Spanish Ministry of Science and Innovation. SEM-EBSD analyses were completed at the CITIUS (University of Seville) and the CIC (Centro de Instrumentación Científica, University of Granada). J. Ramírez-Rico is acknowledged for technical support. Fruitful discussions and comments of José María Tubía, Gabriel Gutiérrez-Alonso, Miguel López-Plaza, Guillermo Corretgé and M. Francisco Pereira are gratefully acknowledged. The manuscript has benefited from the critical reviews and suggestions made by Karel Schulmann and Eric Horsman. We warmly thank William M. Dunne for helpful criticism and valuable editorial comments.

Appendix 1

Most models on magmatic tiling simulate rotation and relative displacement of megacrysts using equations developed by Jeffery (1922) and Ghosh and Ramberg (1976), according to which, the rotation rate ($\dot{\phi}$) of a rigid-ellipse major axis depends on the original axis orientation (ϕ), the flow boundary conditions (including the vorticity and shear strain rate, $\dot{\gamma}$) and ellipse axial ratio (R). Therefore, assuming steady-state flow and constant axial ratio, only those particles that are initially parallel can finally interact as magmatic tiling *s.s.* (i.e., mutually parallel tiled pairs, Fig. A1). Therefore, considering a randomly oriented initial fabric, few tiled pairs would be produced in a sample. A corollary

of this statement is that most interactions between rotating megacrysts within the magma would be non-parallel (Fig. 7). However, general megacryst interactions (not necessarily tiled pairs) could be also used as sense of shear criterion and vorticity gauges. In this work, the mathematical determination of sense of tiling (in two dimensions) proposed by Mulchrone et al. (2005) is broadened to include non-parallel interactions. First, it must be admitted that this method only allows determining with confidence the "sense of interaction" of megacrysts. Sense of shear can only be deduced from a statistically representative number of interactions, as explained below. The sense of tiling can be defined as dextral or sinistral (Blumenfeld and Bouchez, 1988; Mulchrone et al., 2005; Fig. A1a). The procedure to establish this sense of tiling is (Fig. A1b): (1) Determine the centre point of the interacting megacrysts (q and s); (2) construct a vector $\vec{u}$ between q and the central point (r) of the short side of the particle; (3) construct a vector $\vec{v}$ between q and s, considering that $\vec{u}$ and $\vec{v}$ define an acute angle; (4) the sense of interaction (SI) is finally given by the third component of the cross product,

$$\mathrm{SI} = \frac{\vec{u} \times \vec{v}}{|\vec{u} \times \vec{v}|}, \tag{A1}$$

for which $+1$ and -1 indicate dextral and sinistral sense of interaction, respectively. Using the right-hand rule of the cross product, dextral tiling can be understood as follows: with the thumb, middle and index fingers at right angles, the index finger points in the direction of $\vec{u}$, and the middle finger represents $\vec{v}$. Therefore, the thumb points downward. The reverse is true for sinistral tiling. The sense of tiling can be also deduced, graphically, by the rotation sense of $\vec{u}$ towards $\vec{v}$. A clockwise rotation indicates dextral sense and *vice versa*. It is remarkable that, whereas in magmatic tiling, the deduced sense of a given tiled pair is the same, irrespective of the particle where the origin of $\vec{u}$ and $\vec{v}$ is located (Fig. A1b), this status is not always the case when general interacting pairs are considered. More general types of interactions between pairs of megacrysts can be seen in Fig. A2. Depending on the relative position of the interacting megacryst and the major axis orientation of both particles, the deduced senses of interaction using each particle as a reference can be mutually consistent (i.e., both dextral or both sinistral, Fig. 7a, b) or inconsistent (i.e., one dextral and the other sinistral, Fig. 7c). In this work, only mutually consistent interactions have been considered as reliable kinematic indicators. Furthermore, in real magmatic rocks, interactions between more than two particles (interacting groups) are common (Fig. 7d, e). When this behaviour has been the case in a studied sample, each interacting pair was analysed separately so that only unambiguous sense of interaction was computed for the entire group. Groups with unambiguous senses have been considered when at least 75% of interacting pairs within the group show mutually consistent senses (Fig. 7d). Otherwise, the interacting group was dismissed for determining sense of rotation (Fig. 7e).

Once a statistically representative number of interacting groups were analysed (see Mulchrone et al. (2005) for more information about the statistics of crystal tiling) and the percentage of dextral and sinistral interactions were determined, the results are compared with the numerical experiments of Mulchrone et al. (2005) to estimate the shear sense of the flow. Considering the most common sense in the studied sample, the 95% confidence lower and upper limits for the proportion of dextral interaction senses (M_L and M_U) are given by Fleiss (1981), Mulchrone et al. (2005):

$$M_{L/U} = \frac{(2nM + z^2 - 1) \pm \sqrt{z^2 - (2 + 1/n) + 4M[n(1-M)+1]}}{2(n + z^2)}, \tag{A2}$$

where M is the proportion of dextral senses, n is the total sample size and z equals to 1.96, giving the 95% confidence interval for M. M_L is obtained using the negative sign before the root, whereas M_U is obtained using the positive sign.

To estimate the kinematic vorticity from the sense of interaction, the results have to be compared with the mathematical simulations from Mulchrone et al. (2005). To do so, not only the proportion of dextral interactions is needed, but also the average aspect ratio of the rotating megacryst (R) and the spacing (p) among them. Mulchrone et al. (2005) proposed a function that relates crystal fraction (f_c), average aspect ratio of particles and spacing, which could be expressed as:

$$p = \sqrt{\frac{2000000}{\sqrt{3} f_c R}}. \tag{A3}$$

Comparison of the measured data with the curves of Mulchrone et al. (2005) allows estimation of the kinematic vorticity of flow. The statistical procedure enables determining lower, upper and mean vorticity values (W_{kL}, W_{kU} and W_k, respectively).

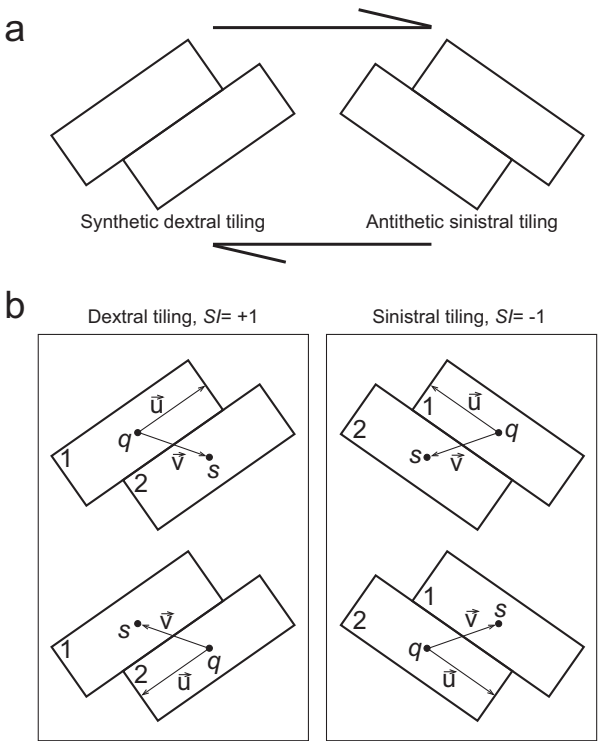

Fig. A1. Criteria to obtain the sense of tiling. Figures modified from Mulchrone et al. (2005). (a) Graphical definition of dextral and sinistral tiling. Tiling is considered synthetic or antithetic with respect to a flow with a component of dextral simple shear. (b) Vector definition of sense of tiling. Left column: dextral tiling. Right column: sinistral tiling. SI: Sense of interaction (Eq. (A1)).

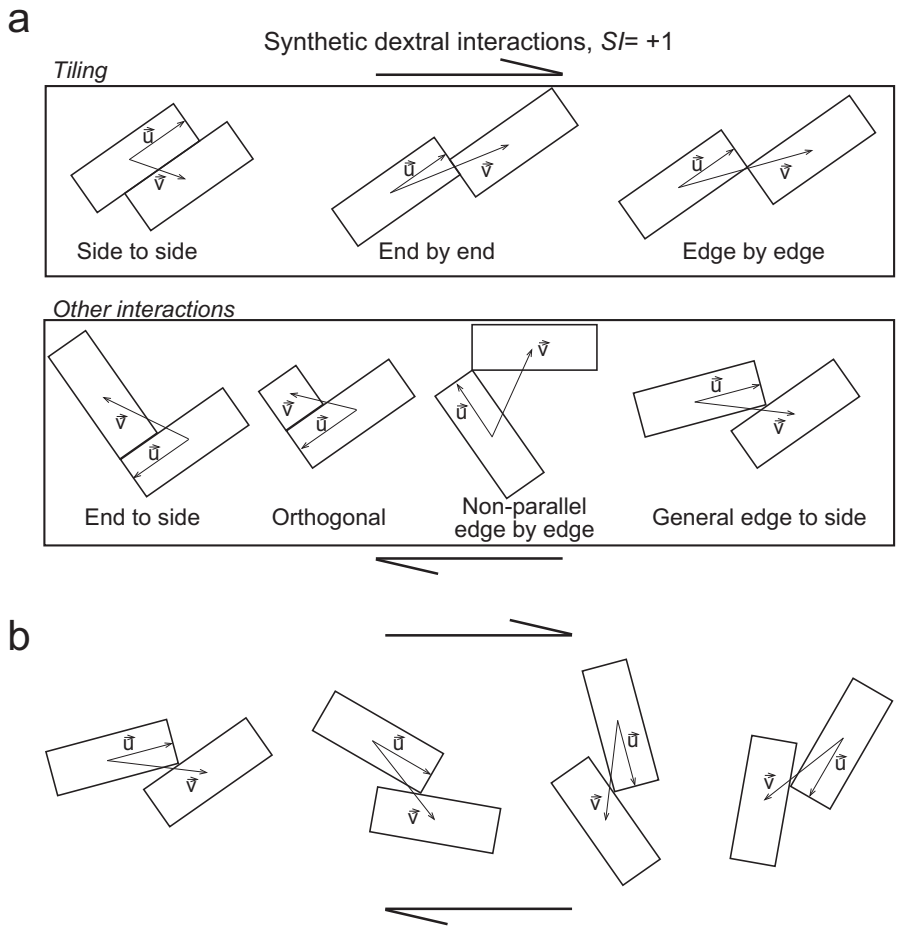

Fig. A2. (a) Distinct types of interactions between megacrysts pairs. Upper row: tiling. Lower row: other types of interactions. All types correspond to dextral interaction. (b) Possible arrangements of a pair of megacrysts with dextral general interaction subjected to a flow with a component of dextral simple shear.

References

Arbaret, L., Fernandez, A., Jezek, J., Ildefonse, B., Launeau, P., Diot, H., 2000. Analogue and numerical modelling of shape fabrics: application to strain and flow determination in magmas. Transactions of the Royal Society of Edinburgh, Earth Sciences 91, 97–109.

Arzi, A.A., 1978. Critical phenomena in the rheology or partially melted rock. Tectonophysics 44, 173–184.

Bea, F., Montero, P., Molina, J.F., 1999. Mafic precursors, peraluminous granitoids, and late lamprophyres in the Avila batholith: a model for the generation of Variscan batholiths in Iberia. Journal of Geology 107, 399–419.

Bea, F., Villaseca, C., Bellido, F., 2004a. El Batolito de Ávila (Sistema Central Español). In: Vera, J.Z. (Ed.), Geología de España. SGE-IGME, Madrid, pp. 101–110.

Bea, F., Montero, P., Zinger, T., 2004b. Edad $^{207}Pb/^{206}Pb$ en cristal único de circón de las rocas máficas y ultramáficas del sector de Gredos, Batolito de Ávila (Sistema Central Español). Revista de la Sociedad Geológica de España 17, 157–167.

Bea, F., Montero, P., González Lodeiro, F., Talavera, C., Molina, J.F., Scarrow, J.H., Whitehouse, M.J., Zinger, T., 2006. Zircon thermometry and U-Pb ion-microprobe dating of the gabbros and associated migmatites of the Variscan Toledo anatectic complex, Central Iberia. Journal of the Geological Society, London 163, 847–855.

Benn, K., Paterson, S.R., Lund, S.P., Pignotta, G.S., Kruse, S., 2001. Magmatic fabrics in batholiths as markers of regional strains and plate kinematics: example of the Cretaceous Mt. Stuart Batholith. Physics and Chemistry of Earth (A) 26, 343–354.

Berger, A.R., Pitcher, W.S., 1970. Structures in granitic rocks: a commentary and critique on granite tectonics. In: Proceedings of the Geological Society, London, vol. 81, pp. 441–461.

Berthé, D., Choukroune, P., Jegouzo, P., 1979. Orthogneisses, mylonite and non-coaxial deformation of granites: the example of the South Armorican shear zone. Journal of Structural Geology 1, 31–42.

Blumenfeld, P., Bouchez, J.L., 1988. Shear criteria in granite and migmatite deformed in the magmatic and solid states. Journal of Structural Geology 10, 361–372.

Bouchez, J.L., 1997. Granite is never isotropic: an introduction to AMS studies of granitic rocks. In: Bouchez, J.L., Hutton, D.H.W., Stephens, W.E. (Eds.), Granite: From Segregation of Melt to Emplacement Fabrics. Kluwer, Dordrecht, pp. 95–112.

Bouchez, J.L., Delas, C., Gleizes, G., Nédélec, A., Cuney, M., 1992. Submagmatic microfractures in granites. Geology 20, 35–38.

Bouchez, J.L., Hutton, D.H.W., Stephens, W.E. (Eds.), 1997. Granite: From Segregation of Melt to Emplacement Fabrics. Kluwer, Dordrecht, p. 358.

Brown, M., 1994. The generation, segregation, ascent and emplacement of granite magma: the migmatite-to-crustally-derived granite connection in thickened orogens. Earth Science Reviews 36, 83–130.

Brown, M., Solar, G.S., 1999. The mechanism of ascent and emplacement of granite magma during transpression: a syntectonic granite paradigm. Tectonophysics 312, 1–33.

Capdevila, R., Corretgé, L.G., Floor, P., 1973. Les granitoides varisques de la Mesete Iberique. Bulletin de la Société Géologique de France 7-15, 209–228.

Caricchi, L., Burlini, L., Ulmer, P., Gerya, T., Vassalli, M., Papale, P., 2007. Non-Newtonian rheology of crystal-bearing magmas and implications for magma ascent dynamics. Earth and Planetary Science Letters 264, 402–419.

Casquet, C., Montero, P., Galindo, C., Bea, F., Lozano, R., 2004. Geocronología $^{207}Pb/^{206}Pb$ en cristal único de circón y Rb-Sr del plutón de La Cabrera (Sierra del Guadarrama). Geogaceta 35, 71–74.

Castiñeiras, P., Villaseca, C., Barbero, L., Martín Romera, C., 2008. SHRIMP U-Pb zircon dating of anatexis in high-grade migmatite complexes of central Spain: implications in the Hercynian evolution of Central Iberia. International Journal of Earth Sciences 97, 35–50.

Castro, A., 1987. On granitoid emplacement and related structures. A review. Geologische Rundschau 76, 101–124.

Castro, A., Fernández, C., Vigneresse, J.L. (Eds.), 1999. Understanding granites: integrating new and classical techniques. Geological Society, London, Special Publication 168, p. 288

Castro, A., Corretgé, L.G., De La Rosa, J., Enrique, P., Martínez, F.J., Pascual, E., Lago, M., Arranz, E., Galé, C., Fernández, C., Donaire, T., López, S., 2002. Paleozoic magmatism. In: Gibbons, W., Moreno, M.T. (Eds.), The Geology of Spain. Geological Society, London, pp. 117–153.

Castro, A., García Casco, A., Fernández, C., Corretgé, L.G., Moreno-Ventas, I., Gerya, T., Löw, I., 2009. Ordovician ferrosilicic magmas: experimental evidence for

ultrahigh temperatures affecting a metagreywacke source. Gondwana Research 16, 622–632.
Clemens, J.D., Mawer, C.K., 1992. Granitic magma transport by fracture propagation. Tectonophysics 204, 339–360.
Clemens, J.D., Petford, N., Mawer, C.K., 1997. Ascent mechanisms of granitic magmas: causes and consequences. In: Holness, M.B. (Ed.), Deformation-Enhanced Fluid Transport in the Earth's Crust and Mantle. Chapman Hall, London, pp. 145–172.
Cloos, H., 1925. Einfurhung in die tectonische Behandlung magmatischer Erscheinungen (Granittektonik). Pt 1: Das Riesengebirge in Shlesien. Gebrüder Borntraeger, Berlin.
Collins, W.J., Sawyer, E.W., 1996. Pervasive granitoid magma transport through the lower-middle crust during non-coaxial compressional deformation. Journal of Metamorphic Geology 14, 565–579.
Dallmeyer, R.D., Martínez Catalán, J.R., Arenas, R., Gil Ibarguchi, J.I., Gutiérrez Alonso, G., Farias, P., Aller, J., Bastida, F., 1997. Diachronous Variscan tectonothermal activity in the NW Iberian Massif: evidence from $^{40}Ar/^{39}Ar$ dating of regional fabrics. Tectonophysics 277, 307–337.
Días, G., Leterrier, J., Mendes, A., Simoes, P.P., Bertrand, J.M., 1998. U-Pb zircon and monazite geochronology of post-collisional Hercynian granitoids from the Central Iberian Zone (Northern Portugal). Lithos 45, 349–369.
Díaz-Alvarado, J., Fernández, C., Moreno-Ventas, I., Castro, A., 2006. Estructura de los cuerpos plutónicos y migmatíticos en la parte central del Macizo de Gredos. Geogaceta 39, 27–30.
Díaz-Alvarado, J., Fernández, C., Díaz Azpiroz, M., Martínez-Rico, J., Moreno-Ventas, I., Castro, A., 2007. Análisis de la microfábrica de cuarzo en los resister cuarcíticos de la zona de cizalla dúctil de la Garganta de las Pozas, parte central del Macizo de Gredos. Geogaceta 43, 31–34.
Díaz-Alvarado, J., Castro, A., Fernández, C., Moreno-Ventas, I., 2011a. Assessing bulk assimilation in cordierite-bearing granitoids from the Central System batholith, Spain; experimental, geochemical and geochronological constraints. Journal of Petrology 52, 223–256.
Díaz-Alvarado, J., Castro, A., Fernández, C., Moreno-Ventas, I., Armstrong, R., 2011b. SHRIMP U-Pb zircon geochronology of intrusive granitoids and anatectic leucogranites in the Gredos Massif, Central System batholith, Spain. Implications of the building of the batholith. Geophysical Research Abstracts 13, EGU2011–6231.
Díez-Balda, M.A., Martínez-Catalán, J.R., Ayarza-Arribas, P., 1995. Syn-collisional extensional collapse parallel to the orogenic trend in a domain of steep tectonics: the Salamanca Detachment Zone (Central Iberian Zone, Spain). Journal of Structural Geology 17, 163–182.
Dingwell, D.B., 1999. Granitic melt viscosities. In: Castro, A., Fernández, C., Vigneresse, J.L. (Eds.), Understanding Granites. Integrating New and Classical Techniques. Geological Society, London, Special Publications 168, pp. 27–38.
Doblas, M., 1991. Late Hercynian extensional and transcurrent tectonics in central Iberia. Tectonophysics 191, 325–334.
D'Lemos, R.S., Brown, M., Strachan, R.A., 1993. Granite magma generation, ascent and emplacement within a transpressional orogen. Journal of the Geological Society, London 149, 487–490.
Escuder Viruete, J., Arenas, R., Martínez Catalán, J.R., 1994. Tectonothermal evolution associated with Variscan crustal extension in the Tormes Gneiss Dome (NW Salamanca, Iberian Massif, Spain). Tectonophysics 238, 1–22.
Escuder Viruete, J., Hernáiz Huerta, P.P., Valverde Vaquero, P., Rodríguez Fernández, R., Dunning, G., 1998. Variscan syncollisional extension in the Iberian Massif: structural, metamorphic and geochronological evidence from the Somosierra sector of the Sierra de Guadarrama (Central Iberian Zone, Spain). Tectonophysics 290, 87–109.
Farina, F., Dini, A., Innocenti, F., Rocchi, S., Westerman, D.S., 2010. Rapid incremental assembly of the Monte Capanne pluton (Elba Island, Tuscany) by downward stacking of magma sheets. Geological Society of America Bulletin 122, 1463–1479.
Faure, M., 1995. Late Carboniferous extensions in the Variscan French Massif Central. Tectonics 14, 132–153.
Fernández, C., Castro, A., 1999. Brittle behaviour of granitic magma: the example of Puente del Congosto, Iberian Massif, Spain. In: Castro, A., Fernández, C., Vigneresse, J.L. (Eds.), Understanding Granites: Integrating New and Classical Techniques. Geological Society, London, Special Publications 168, pp. 191–206.
Fernández, C., Díaz-Azpiroz, M., 2009. Triclinic transpression zones with inclined extrusion. Journal of Structural Geology 31, 1255–1269.
Fernandez, A., Fernández-Catuxo, J., 1997. 3D biotite shape fabric experiments under simple shear strain. In: Bouchez, J.L., Hutton, D.H.W., Stephens, W.E. (Eds.), Granite: From Segregation of Melt to Emplacement Fabrics. Kluwer, Dordrecht, pp. 145–157.
Fernández, C., Becchio, R., Castro, A., Viramonte, J.M., Moreno-Ventas, I., Corretgé, L.G., 2008. Massive generation of atypical ferrosilicic magmas along the Gondwana active margin: implications for cold plumes and back-arc magma generation. Gondwana Research 14, 451–473.
Fleiss, J.L., 1981. Statistical Methods for Rates and Proportions. John Wiley and Sons, New York.
Flinn, D., 1962. On folding during three dimensional progressive deformation. Quarterly Journal of the Geological Society, London 118, 385–428.
Fossen, H., Tikoff, B., 1998. Extended models of transpression and transtension, and application to tectonic settings. In: Holdsworth, R.E., Strachan, R.A., Dewey, J.F. (Eds.), Continental Transpression and Transtension Tectonics. Geological Society, London, Special Publication, vol. 135, pp. 15–33.
Ghosh, S.K., Ramberg, H., 1976. Reorientation of inclusions by combination of pure shear and simple shear. Tectonophysics 34, 1–70.
Giordano, D., Russell, J.K., Dingwell, D.B., 2007. Viscosity of magmatic liquids: a model for volcanology. Geophysical Research. Abstracts 9.
Giorgis, S., Tikoff, B., 2004. Constraints on kinematics and strain from feldspar porphyroclast populations. In: Alsop, G.I., Holdsworth, R.E., McCaffrey, K.J.W., Hand, M. (Eds.), Flow Processes in Faults and Shear Zones. Geological Society, London, Special Publications 224, pp. 265–285.
Gutiérrez-Alonso, G., Murphy, J.B., Fernández-Suárez, J., Weil, A.B., Franco, M.P., Gonzalo, J.C., 2011. Lithospheric delamination in the core of Pangea: Sm-Nd insights from the Iberian mantle. Geology 39, 155–158.
Hess, K.U., Dingwell, D.B., 1996. Viscosities of hydrous leucogranitic metls: a non-Arrhenian model. American Mineralogist 81, 1297–1300.
Higgins, M.D., 2006. Quantitative Textural Measurements in Igneous and Metamorphic Petrology. Cambridge University Press, Cambridge, p. 265.
Holtz, F., Roux, J., Ohlhorst, S., Behrens, H., Schulze, F., 1999. The effects of silica and water on the viscosity of hydrous quartzofeldspathic melts. American Mineralogist 84, 27–36.
Hossack, J.R., 1968. Pebble deformation and thrusting in the Bygdin area (S. Norway). Tectonophysics 5, 315–339.
Jeffery, G.B., 1922. The motion of ellipsoidal particles immersed in a viscous fluid. Proceedings of the Royal Society of London A 102, 201–211.
Jelinek, V., 1981. Characterization of the magnetic fabrics of rocks. Tectonophysics 79, 63–67.
Jessell, M.W., 1988. Simulation of fabric development in recrystallizing aggregates. 2: example model runs. Journal of Structural Geology 10, 779–793.
Jiang, D., 2007. Numerical modelling of the motion of rigid ellipsoidal objects in slow viscous flows: a new approach. Journal of Structural Geology 29, 189–200.
Johnson, B.R., Glazner, A.F., 2010. Formation of K-feldspar megacrysts in granodioritic plutons by thermal cycling and late-stage textural coarsening. Contributions to Mineralogy and Petrology 159, 599–619.
Joly, A., Faure, M., Martelet, G., Chen, Y., 2009. Gravity inversion, AMS and geochronological investigacions of syntectonic granitic plutons in the southern part of the Variscan French Massif Central. Journal of Structural Geology 31, 421–443.
Koenders, M.A., Petford, M., 2000. Quantitative analysis and scaling of sheared granitic magmas. Geophysical Research Letters 27, 1231–1234.
Kratinová, Z., Schulmann, K., Edel, J.B., Jezek, J., Schaltegger, U., 2007. Model of successive granite sheet emplacement in transtensional setting: integrated microstructural and anisotropy of magnetic susceptibility study. Tectonics 26. http://dx.doi.org/10.1029/2006TC002035.
Kratinová, Z., Jezek, J., Schulmann, K., Hrouda, F., Shail, R.K., Lexa, O., 2010. Non-coaxial K-feldspar and AMS subfabrics in the Land's End granite, Cornwall. Evidence of magmatic fabric decoupling during late deformation and matrix crystallization. Journal of Geophysical Research 115, B09104. http://dx.doi.org/10.1029/2009JB006714.
Kratinová, Z., Schulmann, K., Edel, J.B., Tabaud, A.S., 2012. AMS record of brittle dilation, viscous-stretching and gravity-driven magma ascent in area of magma-rich crustal extension (Vosges Mts, NE France). International Journal of Earth Sciences 101, 803–817.
Kretz, R., 1983. Symbols for rock-forming minerals. American Mineralogist 68, 277–279.
Launeau, P., Robin, P.-Y.F., 2005. Determination of fabric and strain ellipsoids from measured sectional ellipses – implementation and applications. Journal of Structural Geology 27, 2223–2233.
Lister, G.S., Hobbs, B.E., 1980. The simulation of fabric development during plastic deformation and its application to quartzite: the influence of deformation history. Journal of Structural Geology 2, 355–371.
Lode, W., 1926. Versuche ubre den Einfluss der mittleren Hauptspannung auf das Fliessen der Metalle Eisen, Kupfer und Nickel. Zeitschrift für Physik 36, 913–939.
Martínez Catalán, J.R., Fernández Suárez, J., Jenner, G.A., Belousova, E., Díez Montes, A., 2004. Provenance constraints from detrital zircon U-Pb ages in the northwestern Iberian Massif: implications for Paleozoic plate configuration and Variscan evolution. Journal of the Geological Society, London 161, 461–473.
Martínez Catalán, J.R., 16 others, 2009. A rootless suture and the loss of the roots of a mountain chain: the Variscan belt of NW Iberia. Comptes Rendus Geoscience 341, 114–126.
Montero, P., Bea, F., Zinger, T.F., Scarrow, J.H., Molina, J.F., Whitehouse, M., 2004. 55 million years of continuous antexis in Central Iberia: single-zircon dating of the Peña Negra Complex. Journal of the Geological Society, London 161, 255–263.
Moore, J.G., Sisson, T.W., 2008. Igneous phenocrystic origin of K-feldspar megacrysts in granitic rocks from the Sierra Nevada batholith. Geosphere 4, 387–400.
Moreno-Ventas, I., Rogers, G., Castro, A., 1995. The role of hybridization in the genesis of Hercynian granitoids in the Gredos massif, Spain: inferences from Sr-Nd isotopes. Contributions to Mineralogy and Petrology 120, 137–149.
Mulchrone, K.F., Grogan, S., De, P., 2005. The relationship between magmatic tiling, fluid flow and crystal fraction. Journal of Structural Geology 27, 179–197.
Nadai, A., 1963. Theory of Flow and Fracture of Solids. McGraw-Hill, New York.
Passchier, C.W., Trouw, R.A.J., 1996. Microtectonics. Springer, Berlin.
Pastor-Galán, D., Gutiérrez-Alonso, G., Weil, A., 2011. Orocline timing through joint analysis: insights from the Ibero-Armorican arc. Tectonophysics 507, 31–46.
Paterson, S.R., Vernon, R.H., Tobisch, O.T., 1989. A review of criteria for the identification of magmatic and tectonic foliations in granitoids. Journal of Structural Geology 11, 349–363.

Paterson, S.R., Fowler, T.K., Schmidt, K.G., Yoshinobu, A.S., Yuan, E.S., Miller, R.B., 1998. Interpreting magmatic fabric patterns in plutons. Lithos 44, 53–82.
Pereira, M.D., 1993. Termobarometría de rocas con la asociación granate - cordierita - biotita; trayectorias P-T en el complejo anatéctico de la Peña Negra (Batolito de Ávila). Implicaciones sobre el metamorfismo hercínico en la Zona Centro Ibérica. Revista de la Sociedad Geológica de España 6, 131–140.
Pereira, M.D., Bea, F., 1994. Cordierite-producing reactions in the Peña Negra complex, Avila batholith, Central Spain: the key role of cordierite in low-pressure anatexis. Canadian Mineralogist 32, 763–780.
Petford, N., 2003. Rheology of granitic magma during ascent and emplacement. Annual Review of Earth and Planetary Sciences 31, 399–427.
Petford, N., Kerr, R.C., Lister, J.R., 1993. Dike transport of granitoid magmas. Geology 21, 845–848.
Petford, N., Cruden, A.R., McCaffrey, K.J.W., Vigneresse, J.L., 2000. Granite magma formation, transport and emplacement in the Earth's crust. Nature 408, 669–673.
Ramsay, J.G., 1967. Folding and Fracturing of Rocks. McGraw-Hill, New York.
Robin, P.-Y.F., 2002. Determination of fabric and strain ellipsoids from measured sectional ellipses – theory. Journal of Structural Geology 24, 531–544.
Rutter, E.H., Neumann, D.H.K., 1995. Experimental deformation of partially molten Westerly granite under fluid-absent conditions, with implications for the extraction of granitic magmas. Journal of Geophysical Research 100, 15697–15715.
Rutter, E.H., Brodie, K.H., Irving, D.H., 2006. Flow of synthetic, wet, partially molten "granite" under undrained conditions: an experimental study. Journal of Geophysical Research 111. http://dx.doi.org/10.1029/2005JB004257.
Scaillet, B., Holtz, F., Pichavant, M., 1997. Rheological properties of granitic magmas in their crystallization range. In: Bouchez, J.L., Hutton, D.H.W., Stephens, W.E. (Eds.), Granite: From Segregation of Melt to Emplacement Fabrics. Kluwer, Dordrecht, pp. 11–29.
Schmid, S.M., Casey, M., 1986. Complete fabric analysis of some commonly observed quartz *c*-axis patterns. Geophysical Monographs 36, 263–286.
Schulmann, K., Jezek, J., 2012. Some remarks on fabric overprints and constrictional AMS fabrics in igneous rocks. International Journal of Earth Sciences 101, 705–714.
Schulmann, K., Jezek, J., Venera, Z., 1997. Perpendicular linear fabrics in granite: markers of combined simple shear and pure shear flows? In: Bouchez, J.L., Hutton, D.H.W., Stephens, W.E. (Eds.), Granite: From Segregation of Melt to Emplacement Fabrics. Kluwer, Dordrecht, pp. 159–176.
Sen, K., Mamtani, M.A., 2006. Magnetic fabric, shape preferred orientation and regional strain in granitic rocks. Journal of Structural Geology 28, 1870–1882.
Talbot, J.Y., Faure, M., Chen, Y., Martelet, G., 2005. Pull-apart emplacement of the Margeride granitic complex (French Massif Central). Implications for the late evolution of the Variscan orogen. Journal of Structural Geology 27, 1610–1629.
Valle Aguado, B., Azevedo, M.R., Schaltegger, U., Martínez Catalán, J.R., Nolan, J., 2005. U-Pb zircon and monazite geochronology of Variscan magmatism related to syn-convergence extension in Central Northern Portugal. Lithos 82, 169–184.
van der Molen, I., Paterson, M.S., 1979. Experimental deformation of partially melted granite. Contributions to Mineralogy and Petrology 70, 299–318.
Vernon, R.H., Paterson, S.R., 2008. How late are K-feldspar megacrysts in granites? Lithos 104, 327–336.
Vigneresse, J.L., Barbey, P., Cuney, M., 1996. Rheological transitions during partial melting and crystallization with application to felsic magma segregation and transfer. Journal of Petrology 37, 1579–1600.
Vigneresse, J.L., Tikoff, B., Améglio, L., 1999. Modification of the regional stress field by magma intrusion and formation of tabular granitic plutons. Tectonophysics 302, 203–224.
Villaseca, C., Downes, H., Pin, C., Barbero, L., 1999. Nature and composition of the lower continental crust in Central Spain and the granulite-granite linkage: Inferences from granulitic xenoliths. Journal of Petrology 40, 1465–1496.
Weil, A., Gutiérrez-Alonso, G., Conan, J., 2010. New time constraints on lithospheric-scale oroclinal bending of the Ibero-Armorican Arc: a paleomagnetic study of earliest Permian rocks from Iberia. Journal of the Geological Society, London 167, 127–143.
Wilson, J., Grocott, J., 1999. The emplacement of the granitic Las Tazas complex, northern Chile: the relationships between local and regional strain. Journal of Structural Geology 21, 1513–1523.
Zák, J., Paterson, S.R., Memeti, V., 2007. Four magmatic fabrics in the Tuolumne batholith, central Sierra Nevada, California (USA): implications for interpreting fabric patterns in plutons and evolution of magma chambers in the upper crust. Geological Society of America Bulletin 119, 184–201.
Zák, J., Verner, K., Tycová, P., 2008. Multiple magmatic fabrics in plutons: an over-looked tool for exploring interactions between magmatic processes and regional deformation? Geological Magazine 145, 537–551.
Zeck, H.P., Wingate, M.T.D., Pooley, G.D., 2007. Ion microprobe U-Pb zircon geochronology of a late tectonic granitic-gabbroic rock complex within the Hercynian Iberian belt. Geological Magazine 144, 157–177.